



Repositorio Institucional de la Universidad Autónoma de Madrid

<https://repositorio.uam.es>

Esta es la **versión de autor** del artículo publicado en:

This is an **author produced version** of a paper published in:

Cancer research 76.15 (2016): 4546-4558

DOI: <http://dx.doi.org/10.1158/0008-5472.CAN-15-3268>

Copyright: © 2016 American Association for Cancer Research

El acceso a la versión del editor puede requerir la suscripción del recurso

Access to the published version may require subscription

DNMT1 inhibition reprograms pancreatic cancer cells via upregulation of the miR-17-92 cluster

Sladjana Zagorac ^{1,2}, Sonia Alcala ^{2,4}, Gustavo Fernandez Bayon ⁵, Tony Bou Kheir ¹,
Matthieu Schoenhals ¹, Anna González-Neira ³, Mario Fernandez Fraga ⁵, Alexandra Aicher ^{1,2},
Christopher Heeschen ^{1,2*}, Bruno Sainz Jr ^{2,4}

¹ Stem Cells in Cancer & Ageing, Barts Cancer Institute, Queen Mary University of London, UK.

² Stem Cells & Cancer Group and ³ Human Genotyping-Cegen Unit, Spanish National Cancer Research Centre (CNIO), Madrid, Spain.

⁴ Department of Biochemistry, Universidad Autónoma, Instituto de Investigaciones Biomédicas "Alberto Sols" CSIC-UAM, Madrid, Spain.

⁵ Cancer Epigenetics Unit, Asturias Central University Hospital, Spanish Council for Scientific Research (CSIC), Oviedo, Spain.

* **Correspondence:** Dr. Christopher Heeschen, MD, PhD, Barts Cancer Institute, Queen Mary University of London, UK, Email: c.heeschen@qmul.ac.uk

Running title: DNMT inhibition reprograms pancreatic cancer stem cells

Key words: PDAC, DNA methylation, DNMT1, Zebularine, cancer stem cells, miR-17-92

Word count – 6069

CONFLICT OF INTEREST

The authors declare no conflict of interest

ABSTRACT

Pancreatic ductal adenocarcinoma (PDAC) and other carcinomas are hierarchically organized with cancer stem cells (CSC) residing at the top of the hierarchy where they drive tumor progression, metastasis and chemoresistance. Since CSC and non-CSC share an identical genetic background, we hypothesize that differences in epigenetics account for the striking functional differences between these two cell populations. Epigenetic mechanisms such as DNA methylation play an important role in maintaining pluripotency and regulating the differentiation of stem cells, but the role of DNA methylation in pancreatic CSC is obscure. In this study, we investigated the genome-wide DNA methylation profile of PDAC CSC and we determined the importance of DNMT methyltransferases for CSC maintenance and tumorigenicity. Using high-throughput methylation analysis, we discovered that sorted CSC have a higher level of DNA methylation, regardless of the heterogeneity or polyclonality of the CSC populations present in the tumors analyzed. Mechanistically, CSC expressed higher DNMT1 levels than non-CSC. Pharmacological or genetic targeting of DNMT1 in CSC reduced their self-renewal and in vivo tumorigenic potential, defining DNMT1 as a candidate CSC therapeutic target. The inhibitory effect we observed was mediated in part through epigenetic reactivation of previously silenced microRNAs, in particular the miR-17-92 cluster. Together our findings indicate that DNA methylation plays an important role in CSC biology, and also provide a rationale to develop epigenetic modulators to target CSC plasticity and improve the poor outcome of PDAC patients.

INTRODUCTION

Pancreatic ductal adenocarcinoma (PDAC) represents the 4th most frequent cause of cancer-related death due to its extreme lethality and current lack of effective treatments (1). As incidence and death rates continue to increase, pancreatic cancer is predicted to become the 2nd most frequent cause of cancer-related death by 2030 (2), making this disease a major unmet priority in public healthcare. While multiple subclonal populations of cancer cells coexist within each tumor and are assumed to drive tumor adaptation and therapeutic failure through Darwinian selection (3), convincing evidence now demonstrates that cancer heterogeneity is also driven by phenotypic and functional heterogeneity within each of these subclones, resulting in a hierarchical tumor organization (4). At the apex of this hierarchy are populations of cancer stem cells (CSCs) capable of self-renewal and long-term *in vivo* tumorigenicity. CSCs give rise to more differentiated progenies (non-CSCs), which, although sharing common mutation profiles, bear distinct and thus most likely epigenetically defined gene expression patterns (5,6).

Identifying the epigenetic mechanisms that are responsible for the acquisition and preservation of these distinct CSC features could open up possibilities for the development of new and more effective therapeutic strategies for PDAC. Unlike genetic mutations, epigenetic changes are transient and reversible, and as such, therapies that convert the epigenetic balance of CSCs towards that of non-CSCs could provide the basis for developing more effective treatment strategies for cancer patients (7). Among the first epigenetic drugs proposed were inhibitors of DNA methylation, e.g. 5-azacytidine (5-aza-CR, azacitidine) and 5-aza-2'-deoxycytidine (5-aza-CdR, Decitabine), followed later by Zebularine, which all incorporate into DNA and form covalent irreversible complexes with DNA methyltransferases (DNMTs) (8). These inhibitors have been shown to induce differentiation of cultured cancer cells (9), but our knowledge about their effects on CSCs is still sparse. Moreover, to date only few studies have utilized the new DNA methylation inhibitor Zebularine, which can be administered orally and is less toxic (10). Thus, we aimed to characterize the supposedly distinct methylation profile of primary pancreatic CSCs and subsequently studied the effects of genetic or pharmacological targeting of DNMT1 on CSC phenotypes.

MATERIAL & METHODS

Primary human cancer cells. PDAC tumors were obtained with written consent from all pancreatic cancer patients, expanded in immunocompromised mice as patient-derived xenografts (PDX), and subsequently digested to establish low-passage primary cell cultures (11).

In vivo tumorigenicity. Serial dilutions of primary pancreatic cancer cells were resuspended in MatrigelTM (BD, Heidelberg, Germany), subcutaneously injected into the right and left flank of female NU-Foxn1^{nu} nude mice (Harlan Laboratories, UK), and tracked for up to 3 months. Experiments were approved by the Animal Experimental Ethics Committee of the Instituto de Salud Carlos III (Madrid, Spain; CBA 68_2013 & CBA 25_2009) and performed in accordance with the guidelines for Ethical Conduct in the Care and Use of Animals. CSC frequency was calculated using the extreme limiting dilution analysis (LDA) algorithm (<http://bioinfo.wehi.edu.au/software/elda/index.html>).

Sphere formation assay. Spheres were generated by culturing 2×10^3 PDAC cells per ml in ultra-low attachment plates (Corning, NY, NY) using serum-free DMEM/F12 supplemented with B27 (1:50, Invitrogen, Waltham, MA), 20ng/ml bFGF, and 50units/ml penicillin/streptomycin for 7 days. For serial passaging, sphere cultures were first depleted for single cells and “spheres” measuring $<40\mu\text{m}$ using a $40\mu\text{m}$ cell strainer. Retained spheres were dissociated into single cells, re-cultured for another 7 days. Spheres $>40\mu\text{m}$ were quantified with a CASY Cell Counter (Roche, Mannheim, Germany) (11). Primary sphere-derived human PDAC cells were treated with Zebularine (75 μM) or Decitabine (50 μM) for 7days. The drugs were re-administered every other day to the cell suspension.

Flow cytometry analysis and FACS sorting. Primary pancreatic cells, dissociated spheres or cells from tumor digestions were stained with anti-hCD133/1-APC or PE (Miltenyi Biotec, Bergisch Gladbach, Germany), hEPCAM-APC (Miltenyi), hCD324-APC (Biolegend, London, UK), hPan-Cytokeratin-FITC (Miltenyi) or appropriate control antibodies (all from BD), counter-stained with DAPI (2 $\mu\text{g/ml}$) for exclusion of dead cells and analyzed using a FACS CANTO II instrument (BD). Data were analyzed with FlowJo 9.2 software (Tree Star, Ashland, OR). For FACS sorting, cells were adjusted to a concentration

of 10^6 cells/ml in sorting buffer (1X PBS; 3% FBS (v/v); 3mM EDTA). DAPI was added to exclude dead cells, and cells were sorted using a FACS Influx instrument (BD).

DNA methylation analysis. Genomic DNA (1 μ g) was treated by bisulfite conversion with the EZ DNA Methylation Kit (D5004, Zymo Research, Orange, CA) according to the manufacturer's recommendations. The HumanMethylation450K BeadChip (Illumina, Inc, San Diego, CA) was used for analysis of genome-wide DNA methylation according to the manufacturer's instructions. To identify differently methylated probes in paired autofluorescent-positive and -negative cells from all tumors, we used limma package (12). Probes were considered to be differentially methylated if the resulting adjusted P-value was <0.05 . The Benjamini–Hochberg method was used to adjust the P-values and ensure that the false discovery rate was <0.05 . The genomic region of the probes from the array were assigned according to their position relative to the transcript information obtained from the R/Bioconductor package FDb.InfiniumMethylation.hg19 (R package version 2.9.2). The CGI locations used in the analyses were obtained from the R/Bioconductor package FDb.InfiniumMethylation.hg19 (R package version 1.0.1). The definition of CGI was done as described previously (13).

Statistical analysis. Results for continuous variables are presented as means \pm SEM unless stated otherwise and significance was determined using the Mann-Whitney U test. All analyses were performed using SPSS 22.0 (SPSS, Chicago, IL). Significance was considered at $p < 0.05$.

Additional experimental details can be found in the Supplementary Materials and Methods.

RESULTS

Pancreatic CSCs bear higher DNA methylation levels. We first performed genome-wide comprehensive methylation profiling using the 450K Illumina bead array (14) in order to gain insight into putative DNA methylation differences between CSCs and non-CSCs. CSCs can be separated from the tumor bulk population by several methods (11); however, we recently showed that PDAC CSCs can also be efficiently isolated using autofluorescence (an accumulation of riboflavin in ATP-dependent

transporter ABCG2-coated vesicles exclusively found in CSCs) (15). Using this CSC inherent marker, we separated CSCs from non-CSCs by FACSsorting (**Figure 1A**) (15), and the efficient enrichment for CSCs was validated by increased expression of pluripotency-associated genes in autofluorescent-positive (Fluo+) CSCs versus Fluo– cells (**Figure S1A/B**).

As the vast intratumoral heterogeneity in PDAC might obscure distinct methylation profiles between CSCs and non-CSCs within each contained subclone we did not only use cells derived from a heterogeneous primary pancreatic tumor (PDAC-185), but also analyzed a liver metastasis (PDAC-A6L), and a single cell-derived (SCD) tumor that was generated using a single CSC isolated from the primary tumor (PDAC-185 SCD) (**Figure S1C/D**). We reasoned that the CSC heterogeneity should be highest in the primary tumor, less in the metastatic tumor and homogenous in the CSCs isolated from the SCD tumor. DNA methylation levels were compared between CSCs and non-CSCs for each individual tumor, which revealed a slight, but significant increase in DNA methylation in the Fluo+ CSC compartment, regardless of the heterogeneity or polyclonality of the CSC populations present (**Figure 1B**). These data suggest consistent differences in the methylation profile despite considerable intratumoral heterogeneity.

Furthermore, we looked at differentially methylated probes (hyper- or hypomethylation) in CSCs and found that their distribution was not universal. Hypermethylation was mostly located in non-CGI (Odds ratio[OD]=1.43) and intergenic regions (OR=1.17) and hypomethylation was mostly found in CGI (OR=1.80) and promoter regions (OR=1.43) (**Figure 1C**), indicating that the hypermethylation phenotype observed in the pancreatic CSC population is largely a result of methylation of regions that are outside of traditional CGI. To further confirm this observation, we measured the levels of the DNA methylation mark 5-methylcytosine (5mC) using the MethylFlash Methylated DNA Kit or by manual dotblot analysis and show that regardless of the method used to isolate CSCs (sphere vs adherent, Fluo+ vs Fluo–, or CD133+ vs CD133–), the CSC population exhibited consistently higher levels of 5mC, indicating that cytosine was methylated to 5-methylcytosine by DNMTs, which is in line with our Illumina Array data (**Figures 1D & S2A**).

Pancreatic cancer stem cells overexpress DNMT1. We next asked if hypermethylation could be explained by differential expression of DNMTs. Most strikingly, we found higher mRNA expression levels of DNMT1 in the CSC population, regardless of the isolation method used (**Figures 2A, 2C & S2B**). Western blot analysis confirmed higher DNMT1 protein expression in CSCs vs non-CSCs (**Figure 2B-D**). Based on the above data, we reasoned that DNMT1 overexpression plays a decisive role in preserving the stemness state of CSCs via maintaining their distinct methylation state (16).

DNMT1 inhibition decreases PDAC CSCs phenotypes. Based on the aforementioned results, we aimed to pharmacologically target DNMT1 using Zebularine (Zeb) in order to reverse the distinct methylome signature of CSCs and assess whether DNMT1 inhibition could ablate PDAC CSC tumorigenicity. Three primary PDAC cell cultures were treated with Zebularine over the course of 7 days in conditions that enrich for CSCs (**Figure S3A/B**). A concentration of 75 μ M was used in all of our subsequent experiments as cytotoxicity studies revealed that concentrations $\geq 100\mu$ M were potentially toxic (**Figure S3C**).

While Zebularine expectedly showed minor or no effect on *DNMT1* mRNA levels (**Figure S3D**), we observed a consistent inhibition of DNMT1 at the protein level (**Figure 3A**) and a marked reduction in CD133 mRNA and surface protein levels (**Figure 3B**), suggesting preferential targeting of CSCs. A similar reduction was observed when we sorted cells for autofluorescence to identify CSCs (**Figure S3E**). At the functional level Zebularine reduced both CSC self-renewal *in vitro* (**Figure 3C**) and the expression of pluripotency-associated genes (**Figure 3D**). To further corroborate that pharmacological inhibition of DNMT1 is suitable for targeting pancreatic CSCs, we used another DNMT inhibitor, Decitabine (DAC). Indeed, non-toxic levels of DAC (**Figure S4A**) decreased DNMT1 protein levels (**Figure S4B**) and subsequently reduced the self-renewal capacity of CSCs in three different PDAC cultures (**Figure S4C**). Moreover, DAC treatment significantly decreased the expression of the pluripotency-associated gene *OCT3/4* (**Figure S4D**). The differential effects on the expression of pluripotency-associated genes between Zebularine and DAC may, at least in part, be related to differences in DNA-hypomethylating

properties of the drugs as previously suggested (17). Nonetheless, at the functional level, both DNMT1 inhibitors significantly inhibited the CSC population. Since the most defining feature of CSCs is their ability to form tumors *in vivo*, we also performed limiting dilution *in vivo* tumorigenicity assays with control or Zebularine-treated cells to assess their tumorigenic potential. Zebularine-treated cells produced significantly fewer (and smaller) tumors resulting in a 5-6-fold lower calculated CSC frequency (**Figure 3E, left panel**). Moreover, in tumors that did form, the percentage of CD133+ cells was markedly reduced (**Figure 3E, right panel**), already suggesting enhanced epithelial differentiation as a possible mechanism of action.

Knockout of DNMT1 decreases CSCs phenotypes. DNMT1 inhibitors, including Zebularine and DAC, have a similar mode of action (incorporation into DNA as cytosine analogues). The formation of covalent adducts between DNA and trapped DNA methyltransferase protein can induce toxic effects, making it difficult to separate demethylating activity from cytotoxicity (18). Therefore, to genetically verify our hypothesis that DNMT1 is indeed crucial for maintaining the CSC status, we generated PDAC cells lacking DNMT1 via CRISPR/Cas9 editing. After two weeks under selection the 185 *DNMT1*-KO cells showed complete loss of DNMT1 expression at the protein level (**Figure 4A**). The subsequent loss of DNMT1 i) decreased the percentage of CD133+ CSCs (**Figure 4B**), ii) significantly abrogated the *in vitro* self-renewal capacity of CSCs as measured by multiple generation sphere-formation potential (**Figure 4C**), and iii) decreased the expression of pluripotency-associated genes (**Figure 4D**).

The DNMT1 inhibition promotes CSC proliferation and differentiation. The effects of DNMT1 inhibition on CSCs may be related to i) apoptosis induction, ii) cell cycle arrest, or iii) promotion of differentiation. Zebularine treatment during sphere formation did not significantly alter the percentage of early or late apoptotic cells in the entire tumor cell population (**Figure 5A, left panel**) nor was there any evidence of apoptosis induction specifically in the CD133+ CSC population (**Figure 5A, right panel**). Cell cycle analysis, however, revealed reduced numbers of Zebularine-treated cells residing in G0 and an increased number of actively cycling cells (**Figure 5B**). Moreover, not only did we observe a decrease in

the percentage of CD133+ CSCs upon treatment (**Figure 3B**), but by comparing ratios between the CD133– and the CD133+ cell populations, we found that the decrease in CD133+ CSCs was followed by an increase in their CD133-negative non-CSC counterparts, suggesting that Zebularine treatment potentially induced the “differentiation” of CSCs to non-CSC (**Figure 5C**). This result was confirmed by assessing the cell surface levels of pan-Cytokeratin and E-cadherin (**Figures 5D-E and S5A-B**) as markers of more differentiated PDAC cells (6). Higher expression of Pan-Cytokeratin and E-Cadherin could also be observed following DAC treatment (**Figure S4E**) and DNMT1 knockout (**Figure S5C**). Together, our data suggest a quiescence inhibiting and differentiation promoting effect of DNMT1 inhibition on pancreatic CSCs.

DNMT1 inhibition affects CSCs via hypomethylation of the miR-17-92 cluster. To determine the molecular mechanism(s) responsible for the effect of Zebularine on CSCs, we analyzed putative changes in DNA methylation using the Illumina Infinium HumanMethylation450 Bead Chip. As expected, Zebularine treatment decreased DNA methylation in PDAC CSCs (**Figure 6A**). Interestingly, while methylation of many genes was changed upon treatment, others even gained methylation. Using a stringent analysis approach (fold change in β -methylation values less than 0.5 and fold change higher than 2) we found 97 and 548 genes demethylated and methylated, respectively (**Tables S1 & S2**). While these genes are currently under investigation, previous work by our group indicated that miRNAs (miR) have an important role in PDAC CSCs, and thus we initially focused our analysis on modulated miR. Indeed, as shown in **Table 1**, we identified several miR more methylated in CSC-enriched spheres versus non-CSC adherent cultures, and using a less stringent analysis (fold change in β -methylation values 0.8) many were subsequently hypomethylated following Zebularine treatment (**Table S3**).

Among these, we identified miR-203 and -205, which have previously been implicated in promoting cellular differentiation (19). While the expression of these miR could not be confirmed to be significantly altered by Zebularine (**Figure S6A**), we did see a strong and significant increase in the expression of these two miR in *DNMT1*-KO cells (**Figure S6B**). Next, we focused our attention on the

miR-17HG (miR-17-92 cluster host gene) as a potentially methylation-regulated miR as Zebularine treatment phenocopied previous data from our laboratory related to the miR-17-92 cluster in CSCs (20). We previously showed that suppression of this cluster was necessary for the maintenance of CSC phenotypes and artificial overexpression of miR17-92 members forces quiescent CSCs into an active cell cycle state (20). Likewise, previous reports have observed a CpG island in close proximity of the miR-17-92 promoter (21). Encouraged by these findings, we further investigate whether hypermethylation of this CpG island could be responsible for the apparent suppression of this important miR cluster in CSC-enriched spheres (20). Indeed, analysis of our methylation array data showed that CpG sites in close proximity of the miR-17-92 cluster were hypomethylated upon Zebularine treatment (**Table S3**). Using an independent set of CSC-enriched samples from various PDAC tumors, we observed a consistent and notable increase in the expression of several miR-17-92 members following Zebularine treatment (**Figure 6B**), with a particular increase in miR-19a and miR-19b. Consistently, the increased expression of miR-17-92 members, in particular miR-19b, was mimicked in cells lacking DNMT1 (**Figure S6C**). Of note, miR-92a, bearing a unique seed sequence distinguishing it from the other miR-17-92 family members, was not modulated by Zebularine treatment (Ctrl vs Zeb: 1.13 ± 0.02 -fold change, n.s.). Known targets of the miR-17-92 cluster, such as *P21* (*CDKN1A*), *TGFBR2*, *ACVR1B* (ALK4), *SMAD2*, and *SMAD4*, have also been implicated in pancreatic CSC phenotypes including self-renewal and chemoresistance (11,20). We found that many of these genes were suppressed upon Zebularine treatment at both the mRNA and (**Figure 6C**) and protein levels (e.g. P21) (**Figure 6D**), recapitulating our previous findings (20), and suggesting that DNMT1 inhibition is capable of unlocking the epigenetic repression of this cluster in CSCs to reactivate repressed ‘anti-CSC’ miR.

It has been shown that the MYC proto-oncogene family is also involved in the transcriptional regulation of miR-17-92 (22). MYC is generally overexpressed in PDAC, but we recently showed that MYC is actually suppressed in pancreatic CSCs (23), which may contribute to the specific reduced expression of the miR-17-92 cluster in these cells. Indeed, our methylation array data indicated that CpG

sites annotated to MYC were more methylated in CSCs (fold change Adh vs Sph: 1.57 ± 0.18), which could be reversed by Zebularine treatment (fold change Ctrl vs Zeb: 0.80 ± 0.02). We consistently found a significant increase in *c-MYC* mRNA levels in CSC-enriched spheres upon treatment with Zebularine (**Figure 6E**).

Finally, in order to provide more conclusive evidence that the effects of DNMT1 inhibition were primarily mediated via reactivation of the miR-17-92 cluster, we performed loss-of-function experiments in the presence or absence of Zebularine. For this purpose, we plated primary PDAC cells in adherent conditions to obtain a predominantly differentiated PDAC culture and treated these cells for 24h with antagomiR targeting the various members of the miR-17-92 cluster to promote “stemness”, as previously described (20). Following antagomiR treatment we next plated the cells in ultra-low adhesion conditions (sphere culture) to foster the expansion of CSCs and then treated cultures with Zebularine to competitively reverse the effects on CSC phenotypes mediated via miR downregulation. Zebularine reversed the antagomiR-mediated enhancement of sphere formation (**Figure 6F**), supporting the conclusion that Zebularine mediates its inhibitory effects on CSCs, at least in part, by inducing the expression of the members of the miR-17-92 cluster, which functions to repress the expression of CSC-promoting genes.

DISCUSSION

Recent advances in our understanding of CSC epigenetics provide important insights into how these cells acquire their specific stem-like characteristics, and at the same time sheds light on how CSCs can be successfully targeted using epigenetic-modifying agents (24). Our data demonstrate that pancreatic CSCs i) bear higher DNA methylation levels, ii) express high levels of the DNMT methyltransferase protein DNMT1 and iii) loose stemness upon pharmacological or genetic inhibition of DNMT1. While previous studies have already shown that DNMTs are overexpressed in other cancer tissues compared to normal tissue (25,26), herein we report specific up-regulation of DNMT1 in PDAC and provide data to support its role as an important epigenetic modifier in pancreatic CSCs. Intriguingly, demethylation of

pancreatic CSCs using the DNMT1 inhibitors Zebularine and Decitabine markedly reduced their CSC functions and properties, an effect that was regulated via DNMT1-mediated demethylation of the miR-17-92 cluster promoter. These data are in line with reports for other cancers where DNMT1 was also found to be essential for the maintenance of stem cells (27,28), but we now also provide a mechanistic link in the context of PDAC by demonstrating the modulation of a crucial miR cluster.

Epigenetic modifications are able to alter gene expression and have been shown to play a crucial role in stem cell function and maintenance (27,29). As CSCs and their more differentiated progenies share the same genetic background, epigenetic changes should account for the striking functional differences between CSCs and their non-tumorigenic progenies. Specifically, we recently demonstrated that even a single CSC could give rise to a tumor that recapitulated the functional heterogeneity of the original parental tumor at the pathological, biological and genetic levels (15). Thus, epigenetics and not genetics must be the underlying drivers of this intraclonal heterogeneity, which is indeed supported by our present finding that the genome of CSCs is hypermethylated compared to non-CSCs. Strikingly, DNA hypermethylation could not only be found in single-CSC-derived tumors that lack intratumoral heterogeneity, but also in tumors derived from metastatic lesions and even highly heterogeneous primary tumors. This finding supports the notion that hypermethylation is a consistent and robust differential factor between pancreatic CSCs and non-CSCs. At the DNA level, this hypermethylation phenotype was restricted to regions outside traditional CpG islands, specifically non-CpG islands and intergenic regions. In general, it has been shown that cancer cells exhibit hypomethylation of intergenic regions (30), which consequently could contribute to activation of transposable elements and genome instability. On the other hand, promoter regions of many CpG islands of tumor suppressor genes become hypermethylated resulting in their loss-of-function (31). Fortunately, using genome-scale methylation-screening approaches we have learned that a fraction of normally methylated CpG islands become hypomethylated and transcriptionally active in cancer cells (32). Moreover, some CpG islands located within the 3' ends of genes (33) and in intergenic regions (34) exhibit hypermethylation in cancer cells. It is still unclear to

what extent methylation of these non-promoter CpG islands might affect gene expression and more importantly what is the subsequent result/phenotype in different populations of cancer cells. While further studies are necessary to address these specific questions in the context of CSCs, our data allude to a possible mechanism by which PDAC CSCs may protect their genome from undesirable transcription or instability, achieving better fitness for survival and growth than their more differentiated non-CSC counterparts.

DNA methylation is evolutionarily ancient and associated with gene silencing in eukaryotes. It represents a key regulatory mechanism for the self-renewal and differentiation programs of embryonic stem cells (ESC) and of adult stem cells (35). Maintenance of their “stemness” state is conferred to the set of developmental transcription factors (*OCT4*, *NANOG*, and *SOX2*), occupying promoters of genes associated with self-renewal. Expression of these transcriptional regulators is usually controlled by CpG promoter methylation, and differentiation is accomplished by partial or full methylation of pluripotency-associated genes resulting in their downregulation (36). Thus, it is conceivable to predict that treatment of CSCs with de-methylating agents would further up-regulate pluripotency-associated gene expression; however, we observed a downregulation of pluripotency factors indicating that the epigenetic wiring of CSCs is not only different than stem cells but that other epigenetic regulators are likely shaping the epigenetic landscape of CSCs.

Zebularine, a cytidine analog, acts primarily as a trap for DNMT proteins by forming tight covalent complexes between DNMT proteins and DNA after Zebularine incorporation (10). It is believed that the anti-tumor effects of DNMT inhibitors, such as Zebularine or Decitabine, are largely due to the re-expression of tumor suppressor genes (37), which are often silenced in cancer cells. Indeed, we observed that treatment with Zebularine was able to alter methylation patterns of a number of genes in PDAC CSCs including miR genes, which are regulated by methylation and are known to be involved in a wide range of biological processes, including stem cell differentiation (29). In addition, several miR have been shown to be involved in promoting/maintaining stemness in cancers. For example, miR-145 and

miR-9, both well-known tumor-suppressors, were found to be suppressed in several human cancers (38) due to aberrant DNA methylation of their promoters. Thus, we sought to focus our investigation on miR genes and to identify specific CpG sites located in the proximity of various miR promoter regions in which Zebularine-mediated hypomethylation re-activated genes that were originally silenced in CSCs. We observed that the miR-17-92 cluster (comprised of six members – miR17, 18a, 19a, 19b, 20a and 92a) was hypermethylated in CSCs vs non-CSCs (**Table 1**). This finding is in line with recent studies from our laboratory showing that the miR-17-92 cluster is consistently downregulated in pancreatic CSCs (20). In this study we showed that gain-of-function, using forced overexpression of miR-17-92, reduced CSC self-renewal capacity, *in vivo* tumorigenicity and chemoresistance. On the other hand, downregulation of this cluster (i.e. inhibition of miR-17-92 using antagomiR) in more differentiated cells had the opposite effect, imparting non-CSCs with CSC-like phenotypes. This effect was mediated by suppressing multiple members of the *NODAL/ACTIVIN/TGF- β 1* signaling cascade as well as downstream targets, such as *P21*, *P57*, and *TBX3*, all of which have been shown to be crucial for maintaining the stem-like state of pancreatic CSCs (11,20,39). Our data now further validate and expand upon these previous findings and provide novel insights into the epigenetic mechanism(s) controlling the suppression of the miR-17-92 cluster in CSCs. We show, using different approaches, that re-activation of the miR-17-92 cluster following DNMT1 pharmacological or genetic inhibition augments the phenotype of PDAC CSCs.

Unlike other DNMT inhibitors, Zebularine is more stable in aqueous solution and is less toxic *in vitro* and *in vivo* (40). Continuous exposure of various cancer cell lines to Zebularine has already been shown to selectively slow tumor cell growth, highlighting its potential value as a chemotherapeutic agent. It has previously been shown that Zebularine has anti-cancer effects in established PDAC cell lines, supposedly via induction of apoptosis and subsequent suppression of tumor growth *in vivo* (41); however, using primary low-passage PDAC cultures derived from equally low-passage PDX tumors we found no evidence for a direct pro-apoptotic effect. Instead, we show that Zebularine treatment forces normally slow-cycling CSCs into a more proliferative fast-cycling state, which has been previously linked to

chemosensitization via enhanced expression of miR-17-92 (42). Moreover, we observed a marked promotion of CSC differentiation as determined by the loss of “stemness” markers (e.g. CD133) and a gain in the expression of differentiation markers including CYTOKERATIN and E-CADHERIN. More importantly, these phenotypes were recapitulated using not only a different DNMT inhibitor, Decitabine, but also in *DNMT1*-KO cells, indicating that regardless of the approach used, the loss of DNMT1 results in the same phenotypic changes: loss of “stemness” and promotion of differentiation.

We would like to highlight that we cannot exclude the possibility that other CSC inhibitory miR could be reactivated by Zebularine treatment (or DNMT1 inhibition). Indeed **Table S3** shows that upon treatment with Zebularine, β methylation values of various miR genes were decreased. Based on this list and after careful review of the literature, we opted to focus on the two miR, miR-203 and miR-205, as both miR were previously described to play a role in the biology of pancreatic cancer (43,44). miR-203 acts as a known suppressor of stem cell pluripotent factors; therefore, reactivation of miR-203 by hypomethylation might contribute to the reduced levels of pluripotency-associated genes observed following Zebularine treatment in PDAC CSCs. Overexpression of miR-203 has also been demonstrated to induce expression of E-CADHERIN by inhibition of the E-CADHERIN repressors ZEB1/2, which correlates well with our E-CADHERIN immunofluorescence studies presented herein (45). Thus, the pro-differentiation effect of Zebularine can also be potentially explained by Zebularine-induced hypomethylation of miR-203, which has previously been described as an epithelial differentiation factor (19). Likewise, miR-205 is a well-known anti-cancer miR and is consistently downregulated in clinical pancreatic cancer samples including CSCs (44,46). miR-205 replenishment reduces the expression of the pluripotency/stem cell marker OCT3/4, the CSC marker CD44, and resensitizes cells to chemotherapy. Based on these findings we checked the expression of miR-203 and miR-205 in PDAC cells treated with Zebularine and deficient in DNMT1 (i.e. *DNMT1*-KO cells). While expression of these miR was not significantly changed during short-term treatment with Zebularine (**Figure S6A**), we noticed a strong and significant increase in *DNMT1*-KO cells (**Figure S6B**), suggesting that more potent and/or long-term

inhibition of DNMT1 is necessary for miR-203 and miR-205 reactivation. Collectively, we cannot exclude the possibility that other anti-CSCs miR could be reactivated following DNMT1 inhibition; however, our data support the hypothesis that reactivation of the miR-17-92 cluster is a dominating driving factor responsible for the inhibitory effects observed in the PDAC CSC population.

We are still far from thoroughly understanding the role of DNMT1 in the context of CSC biology. Increasing evidence already suggests that DNMT1 protein expression promotes the development of PDAC, from normal tissue to pre-cancerous lesions (PanINs) to PDAC (47). Moreover, DNMT1 has been demonstrated to be essential for the maintenance of hematopoietic stem cells (HSCs)/progenitor cells (48), epidermal progenitor cells and leukemia stem cells (49). More recently, DNMT1 was also shown to be indispensable for mammary stem/progenitor cells and CSC maintenance, and functional inactivation of this gene drastically reduces mammary tumor formation (50). The sum of prior evidence and new insights from our study certainly highlight the important role that DNMT1 plays in cancer biology and at the same time support the continued development of more effective methylation inhibitors as a means of improving the clinical outcome of PDAC patients.

FINANCIAL SUPPORT

Research was supported by the ERC Advanced Investigator Grant (Pa-CSC 233460 to C. Heeschen) and the European Community's Seventh Framework Programme (FP7/2007-2013) under grant agreement n° 256974 (EPC-TM-NET to C. Heeschen) and n° 602783 (CAM-PaC to C. Heeschen), the 2015 SU2C Lustgarten CRUK Pancreatic Cancer Dream Team Award (to C. Heeschen), Pancreatic Cancer UK RIF2014_04 and RIF2015_03 (both to C. Heeschen), a Ramón y Cajal Merit Award from the Ministerio de Economía y Competitividad, Spain (to B. Sainz), a Clinic and Laboratory Integration Program (CLIP) grant from the Cancer Research Institute, NY, NY USA (to B. Sainz) and a Proyecto de Investigación de Salud, ISCIII, Spain (n° PI15/01507 to B. Sainz).

REFERENCES

1. Siegel R, Naishadham D, Jemal A. Cancer statistics, 2012. *CA Cancer J Clin* 2012;62(1):10-29.
2. Rahib L, Smith BD, Aizenberg R, Rosenzweig AB, Fleshman JM, Matrisian LM. Projecting cancer incidence and deaths to 2030: the unexpected burden of thyroid, liver, and pancreas cancers in the United States. *Cancer Res* 2014;74(11):2913-21.
3. Gerlinger M, Rowan AJ, Horswell S, Larkin J, Endesfelder D, Gronroos E, et al. Intratumor heterogeneity and branched evolution revealed by multiregion sequencing. *N Engl J Med* 2012;366(10):883-92.
4. Garcia-Silva S, Frias-Aldeguer J, Heeschen C. Stem cells & pancreatic cancer. *Pancreatology* 2013;13(2):110-3.
5. Visvader JE, Lindeman GJ. Cancer stem cells: current status and evolving complexities. *Cell Stem Cell* 2012;10(6):717-28.
6. Hermann PC, Huber SL, Herrler T, Aicher A, Ellwart JW, Guba M, et al. Distinct populations of cancer stem cells determine tumor growth and metastatic activity in human pancreatic cancer. *Cell Stem Cell* 2007;1(3):313-23.
7. Yoo CB, Jones PA. Epigenetic therapy of cancer: past, present and future. *Nat Rev Drug Discov* 2006;5(1):37-50.
8. Borodovsky A, Salmasi V, Turcan S, Fabius AW, Baia GS, Eberhart CG, et al. 5-azacytidine reduces methylation, promotes differentiation and induces tumor regression in a patient-derived IDH1 mutant glioma xenograft. *Oncotarget* 2013;4(10):1737-47.
9. Constantinides PG, Jones PA, Gevers W. Functional striated muscle cells from non-myoblast precursors following 5-azacytidine treatment. *Nature* 1977;267(5609):364-6.
10. Cheng JC, Yoo CB, Weisenberger DJ, Chuang J, Wozniak C, Liang G, et al. Preferential response of cancer cells to zebularine. *Cancer Cell* 2004;6(2):151-8.
11. Lonardo E, Hermann PC, Mueller MT, Huber S, Balic A, Miranda-Lorenzo I, et al. Nodal/Activin signaling drives self-renewal and tumorigenicity of pancreatic cancer stem cells and provides a target for combined drug therapy. *Cell Stem Cell* 2011;9(5):433-46.
12. Smyth G. limma: Linear Models for Microarray Data. *Statistics for Biology and Health* 2005;Chapter Bioinformatics and Computational Biology Solutions Using R and Bioconductor: 397-420.
13. Wu H, Caffo B, Jaffee HA, Irizarry RA, Feinberg AP. Redefining CpG islands using hidden Markov models. *Biostatistics* 2010;11(3):499-514.
14. Wang T, Guan W, Lin J, Boutaoui N, Canino G, Luo J, et al. A systematic study of normalization methods for Infinium 450K methylation data using whole-genome bisulfite sequencing data. *Epigenetics* 2015;10(7):662-9.
15. Miranda-Lorenzo I, Dorado J, Lonardo E, Alcalá S, Serrano AG, Clausell-Tormos J, et al. Intracellular autofluorescence: a biomarker for epithelial cancer stem cells. *Nat Methods* 2014;11(11):1161-9.
16. Jeltsch A, Jurkowska RZ. New concepts in DNA methylation. *Trends Biochem Sci* 2014;39(7):310-8.
17. Flotho C, Claus R, Batz C, Schneider M, Sandrock I, Ihde S, et al. The DNA methyltransferase inhibitors azacitidine, decitabine and zebularine exert differential effects on cancer gene expression in acute myeloid leukemia cells. *Leukemia* 2009;23(6):1019-28.

18. Juttermann R, Li E, Jaenisch R. Toxicity of 5-aza-2'-deoxycytidine to mammalian cells is mediated primarily by covalent trapping of DNA methyltransferase rather than DNA demethylation. *Proc Natl Acad Sci U S A* 1994;91(25):11797-801.
19. Taube JH, Malouf GG, Lu E, Sphyris N, Vijay V, Ramachandran PP, et al. Epigenetic silencing of microRNA-203 is required for EMT and cancer stem cell properties. *Scientific reports* 2013;3:2687.
20. Cioffi M, Trabulo SM, Sanchez-Ripoll Y, Miranda-Lorenzo I, Lonardo E, Dorado J, et al. The miR-17-92 cluster counteracts quiescence and chemoresistance in a distinct subpopulation of pancreatic cancer stem cells. *Gut* 2015.
21. Ozsolak F, Poling LL, Wang Z, Liu H, Liu XS, Roeder RG, et al. Chromatin structure analyses identify miRNA promoters. *Genes Dev* 2008;22(22):3172-83.
22. O'Donnell KA, Wentzel EA, Zeller KI, Dang CV, Mendell JT. c-Myc-regulated microRNAs modulate E2F1 expression. *Nature* 2005;435(7043):839-43.
23. Sancho P, Burgos-Ramos E, Tavera A, Bou Kheir T, Jagust P, Schoenhals M, et al. MYC/PGC-1alpha Balance Determines the Metabolic Phenotype and Plasticity of Pancreatic Cancer Stem Cells. *Cell Metab* 2015.
24. Wongtrakongate P. Epigenetic therapy of cancer stem and progenitor cells by targeting DNA methylation machineries. *World J Stem Cells* 2015;7(1):137-48.
25. Patra SK, Patra A, Zhao H, Dahiya R. DNA methyltransferase and demethylase in human prostate cancer. *Molecular carcinogenesis* 2002;33(3):163-71.
26. Oh BK, Kim H, Park HJ, Shim YH, Choi J, Park C, et al. DNA methyltransferase expression and DNA methylation in human hepatocellular carcinoma and their clinicopathological correlation. *Int J Mol Med* 2007;20(1):65-73.
27. Broske AM, Vockentanz L, Kharazi S, Huska MR, Mancini E, Scheller M, et al. DNA methylation protects hematopoietic stem cell multipotency from myeloerythroid restriction. *Nat Genet* 2009;41(11):1207-15.
28. Morita R, Hirohashi Y, Suzuki H, Takahashi A, Tamura Y, Kanaseki T, et al. DNA methyltransferase 1 is essential for initiation of the colon cancers. *Exp Mol Pathol* 2013;94(2):322-9.
29. Gangaraju VK, Lin H. MicroRNAs: key regulators of stem cells. *Nature reviews Molecular cell biology* 2009;10(2):116-25.
30. Feinberg AP, Gehrke CW, Kuo KC, Ehrlich M. Reduced genomic 5-methylcytosine content in human colonic neoplasia. *Cancer Res* 1988;48(5):1159-61.
31. Howard G, Eiges R, Gaudet F, Jaenisch R, Eden A. Activation and transposition of endogenous retroviral elements in hypomethylation induced tumors in mice. *Oncogene* 2008;27(3):404-8.
32. Shen L, Kondo Y, Guo Y, Zhang J, Zhang L, Ahmed S, et al. Genome-wide profiling of DNA methylation reveals a class of normally methylated CpG island promoters. *PLoS genetics* 2007;3(10):2023-36.
33. Smith JF, Mahmood S, Song F, Morrow A, Smiraglia D, Zhang X, et al. Identification of DNA methylation in 3' genomic regions that are associated with upregulation of gene expression in colorectal cancer. *Epigenetics* 2007;2(3):161-72.
34. Weber M, Davies JJ, Wittig D, Oakeley EJ, Haase M, Lam WL, et al. Chromosome-wide and promoter-specific analyses identify sites of differential DNA methylation in normal and transformed human cells. *Nat Genet* 2005;37(8):853-62.
35. Bird A. DNA methylation patterns and epigenetic memory. *Genes Dev* 2002;16(1):6-21.

36. Berdasco M, Esteller M. DNA methylation in stem cell renewal and multipotency. *Stem Cell Res Ther* 2011;2(5):42.
37. Christman JK. 5-Azacytidine and 5-aza-2'-deoxycytidine as inhibitors of DNA methylation: mechanistic studies and their implications for cancer therapy. *Oncogene* 2002;21(35):5483-95.
38. Suh SO, Chen Y, Zaman MS, Hirata H, Yamamura S, Shahryari V, et al. MicroRNA-145 is regulated by DNA methylation and p53 gene mutation in prostate cancer. *Carcinogenesis* 2011;32(5):772-8.
39. Lonardo E, Frias-Aldeguer J, Hermann PC, Heeschen C. Pancreatic stellate cells form a niche for cancer stem cells and promote their self-renewal and invasiveness. *Cell Cycle* 2012;11(7):1282-90.
40. Valenzuela MM, Neidigh JW, Wall NR. Antimetabolite Treatment for Pancreatic Cancer. *Chemotherapy (Los Angel)* 2014;3(3).
41. Neureiter D, Zopf S, Leu T, Dietze O, Hauser-Kronberger C, Hahn EG, et al. Apoptosis, proliferation and differentiation patterns are influenced by Zebularine and SAHA in pancreatic cancer models. *Scand J Gastroenterol* 2007;42(1):103-16.
42. Andrade AF, Borges KS, Castro-Gamero AM, Silveira VS, Suazo VK, Oliveira JC, et al. Zebularine induces chemosensitization to methotrexate and efficiently decreases AhR gene methylation in childhood acute lymphoblastic leukemia cells. *Anticancer Drugs* 2014;25(1):72-81.
43. Xu D, Wang Q, An Y, Xu L. MiR203 regulates the proliferation, apoptosis and cell cycle progression of pancreatic cancer cells by targeting Survivin. *Mol Med Rep* 2013;8(2):379-84.
44. Singh S, Chitkara D, Kumar V, Behrman SW, Mahato RI. miRNA profiling in pancreatic cancer and restoration of chemosensitivity. *Cancer Lett* 2013;334(2):211-20.
45. Park SM, Gaur AB, Lengyel E, Peter ME. The miR-200 family determines the epithelial phenotype of cancer cells by targeting the E-cadherin repressors ZEB1 and ZEB2. *Genes Dev* 2008;22(7):894-907.
46. Xu Y, Brenn T, Brown ER, Doherty V, Melton DW. Differential expression of microRNAs during melanoma progression: miR-200c, miR-205 and miR-211 are downregulated in melanoma and act as tumour suppressors. *Br J Cancer* 2012;106(3):553-61.
47. Peng DF, Kanai Y, Sawada M, Ushijima S, Hiraoka N, Kosuge T, et al. Increased DNA methyltransferase 1 (DNMT1) protein expression in precancerous conditions and ductal carcinomas of the pancreas. *Cancer Sci* 2005;96(7):403-8.
48. Trowbridge JJ, Snow JW, Kim J, Orkin SH. DNA methyltransferase 1 is essential for and uniquely regulates hematopoietic stem and progenitor cells. *Cell Stem Cell* 2009;5(4):442-9.
49. Trowbridge JJ, Sinha AU, Zhu N, Li M, Armstrong SA, Orkin SH. Haploinsufficiency of Dnmt1 impairs leukemia stem cell function through derepression of bivalent chromatin domains. *Genes Dev* 2012;26(4):344-9.
50. Pathania R, Ramachandran S, Elangovan S, Padia R, Yang P, Cinghu S, et al. DNMT1 is essential for mammary and cancer stem cell maintenance and tumorigenesis. *Nat Commun* 2015;6:6910.

Table 1 – Hypermethylated miRs in CSC-enriched spheres

has-miRNA	FC_sph vs. adh
hsa-miR548N	1.45
hsa-miR1281	1.42
hsa-miR1259	1.41
hsa-miR1225	1.40
hsa-miR130B/hsa-miR301B	1.40
hsa-miR17HG	1.34
hsa-miR1224	1.31
hsa-miR22	1.26
hsa-miR1227	1.26
hsa-miR1226	1.25
hsa-miR330	1.24
hsa-miR135B	1.24
hsa-miR585	1.21
hsa-miR600	1.21
hsa-miR375	1.20

Given is the Fold Change (FC) of β -methylation values for spheres (sph) vs adherent (adh). Only data for $FC \geq 1.20$ are shown.

FIGURE LEGENDS

Figure 1 – Pancreatic CSCs bear higher levels of DNA methylation. (A) Flow cytometry analysis of autofluorescence in sphere-derived cells from PDAC-185 SCD (PDAC tumor derived from a single PDAC 185 autofluorescent cell), PDAC-185 (primary tumor), and PDAC-A6L (PDAC liver metastasis). (B) Box plots representing DNA methylation levels in representative pairs of autofluorescent-negative and -positive cells from the indicated primary PDAC sphere-derived cultures (* $P < 0.05$). (C) Distribution of differently methylated (M) probes based on their genomic location relative to CpG islands (CGI; **upper panel**). CpG island shores represent regions 0-2 kb from CpG islands, shelves indicate regions 2-4 kb from CpG islands. Distribution relative to the promoter (upstream the transcription start site), and intragenic and intergenic non-promoter regions (**lower panel**). (D) Quantification of 5mC using The MethylFlash™ Quantification Kit in non-CSCs vs CSCs (adh vs sph, Fluo– vs Fluo+, and CD133– vs. CD133+). Data are shown as fold change compared to non-CSC (mean \pm SD; n=3).

Figure 2 – Pancreatic CSCs overexpress DNMT1. (A) qRT-PCR analysis of *DNMT1* mRNA in PDAC adherent (adh) and sphere (sph) cultures. Data are normalized to β -actin levels and represent pooled values from different primary PDAC cultures (A6L, 185, 354, and 215; * $P < 0.05$; n=5). (B) Representative Western blot images of DNMT1 protein expression in a panel of different primary adherent and sphere-derived cultures (A6L, 185 and 354) and densitometric quantification (Quant.) (**left panel**). Changes in protein levels are depicted as fold change in pooled adherent cultures vs pooled sphere-derived cultures (* $P < 0.05$; n=3). (C) Relative mRNA level of *DNMT1* in CSCs (Fluo+ and CD133+) vs non-CSCs (Fluo– and CD133–; * $p < 0.05$, n=3) (**right panel**). (D) Representative Western blot images of DNMT1 protein expression in CSCs (CD133 positive) vs non-CSCs (CD133 negative) and densitometric quantification.

Figure 3 – The DNMT1 inhibitor Zebularine decreases CSC phenotypes. (A) Scheme showing treatment strategy for Control (Ctrl) vs Zebularine (Zeb) in spheres (PDAC-A6L, -185, and -

354) **(left)** and Western blot analysis of DNMT1 protein levels following treatment **(middle)**. Densitometric quantification analysis **(right)** (* $P < 0.05$; $n = 3$). **(B)** qRT-PCR analysis of *CD133* mRNA in PDAC sphere-derived cultures treated with Zebularine for 7 days. Data are normalized to β -actin and represented as fold change compared to untreated cells **(left)** (* $P < 0.05$; $n = 3$). Representative flow cytometry showing the percentage of CD133-positive and -negative cells from PDAC spheres treated for 7 days with Zebularine **(right)**. **(C)** Number of spheres per ml in 1st and 2nd generation cultures from primary PDAC tumors (A6L, 185 and 354; * $P < 0.05$; $n = 4$). **(D)** qRT-PCR analysis of pluripotency-associated genes in 1st generation spheres. Data are normalized to β -actin and presented as fold change in comparison to untreated cells (* $P < 0.05$; $n = 4$). **(E)** Summary of *in vivo* tumorigenicity of subcutaneously injected Control and Zebularine-treated sphere-derived cells 12 weeks post-injection **(left)**. CSC frequencies were determined using the extreme LDA algorithm. Representative flow cytometry plots showing the percentage of CD133 expression in digested tumors derived from Control and Zebularine-treated cells **(right)**.

Figure 4 – Knockout of DNMT1 decreases CSC phenotypes. **(A)** Western blot analysis of DNMT1 protein levels in Control (Cas9) and *DNMT1*-KO cells and densitometric quantification. **(B)** Representative flow cytometry plots of CD133 cell surface expression in Control (Cas9) and *DNMT1*-KO cells. **(C)** Representative images of spheres **(left)** and sphere counts **(right)** in 1st and 2nd generation in Control (Cas9) and *DNMT1*-KO cells (* $P < 0.05$; $n = 3$). **(D)** qRT-PCR analysis of pluripotency-associated genes in *DNMT1*-KO cells. Data are normalized to β -actin and presented as fold change in comparison to Control (Cas9) cells (* $P < 0.05$; $n = 4$).

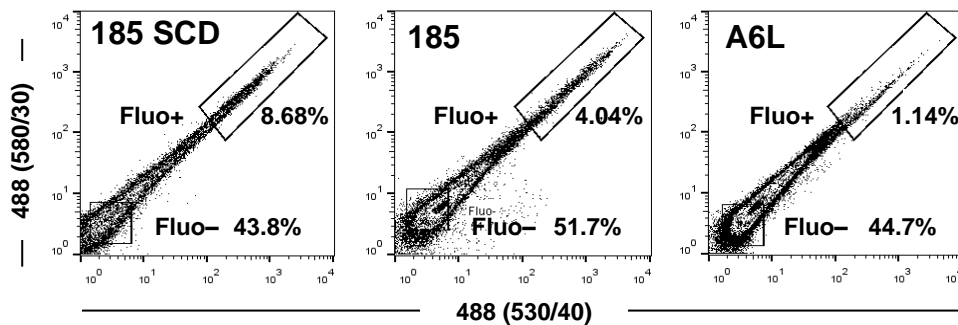
Figure 5 – Zebularine promotes CSC proliferation and differentiation. **(A)** Scheme of the treatment time course **(left)**, AnnexinV expression in Control (Ctrl) and Zebularine (Zeb)-treated PDAC-185, PDAC-354, and PDAC-A6L ($n = 3$) **(middle)**. AnnexinV expression determined within the CD133+ and CD133– fractions, using CD133-PE, for Zeb- and Ctrl-treated PDAC-185, PDAC-354 and PDAC-A6L cultures **(right)**. **(B)** Representative flow cytometry plots for Ki-67 staining in Control vs

Zebularine-treated PDAC-354 cultures (**left panel**) and combined quantification (**right panel**) (* $P < 0.05$; $n = 6$). (**C**) Quantification of flow cytometry analysis of CD133 expression in Control vs Zebularine-treated spheres from PDAC-185 and PDAC-A6L (* $P < 0.05$; $n = 3$). (**D**) Quantification of the mean fluorescence intensity (MFI) of pan-CYTOKERATIN (pan-CK) staining in Control vs Zebularine-treated primary PDAC cultures (**left**) (* $P < 0.05$; $n = 8$). Representative confocal images are shown (**right**). (**E**) Representative confocal images of E-CADHERIN staining for Control vs Zebularine-treated cultures.

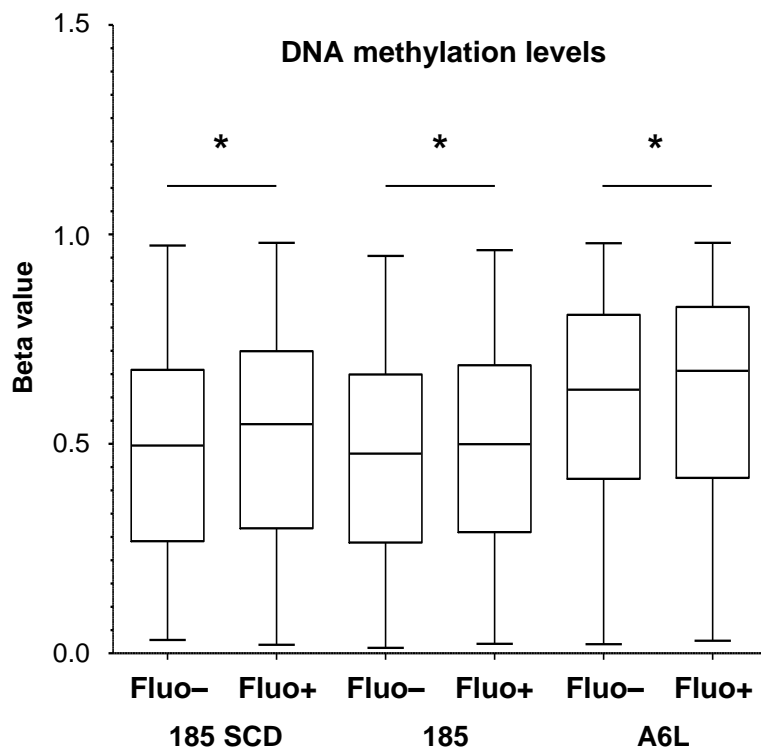
Figure 6 – The effect of Zebularine is mediated via hypomethylation of the miR-17-92 cluster. (**A**) Box plots representing the decrease in DNA methylation levels in pooled Control vs Zebularine-treated PDAC cultures. * $P < 0.05$. (**B**) qRT-PCR analysis of members of the miR-17-92 cluster (miR17, 18a, 19a, 19b, 20a) in PDAC-A6L and PDAC-185 sphere-derived cultures (* $p < 0.05$; $n = 4$). (**C**) qRT-PCR analysis of miR-17-92 target genes in PDAC-A6L and PDAC-185 sphere-derived cultures. Data are normalized to β -actin levels and represented as fold change compared to untreated cells (* $P < 0.05$; $n = 3$). (**D**) Western blot analysis of P21 protein levels in Control vs Zebularine-treated cultures (**upper panel**) and subsequent densitometric quantification (**lower panel**). Changes in protein levels are represented as fold change compared to untreated cells. (**E**) qRT-PCR analysis for *MYC* expression in PDAC-185 cells. Data are normalized to β -actin and represented as fold change in comparison to untreated cells (* $P < 0.05$; $n = 4$). (**F**) PDAC adherent cells were treated with antagomiR for miR-17, 18a, 19a/b, and 20a for 24h. Cells were plated for sphere formation assay, treated with Zebularine for 7 days, and number of spheres per ml were determined (* $P < 0.05$; $n = 6$).

Figure 1 – Pancreatic CSCs bear higher levels of DNA methylation

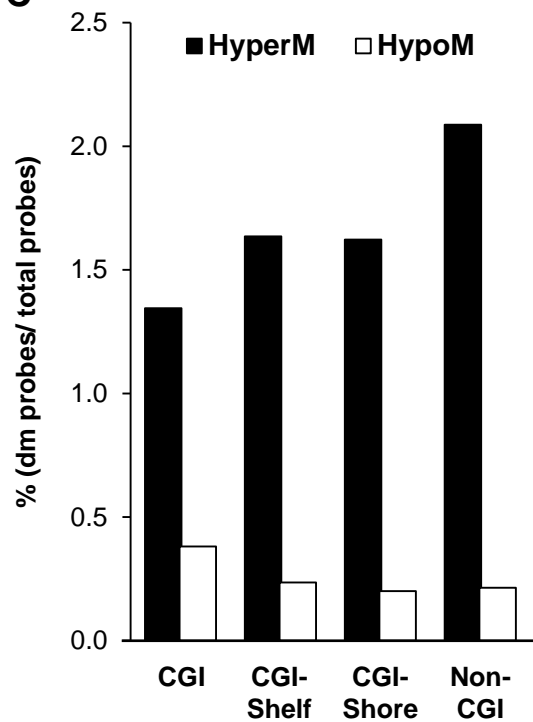
A



B



C



D

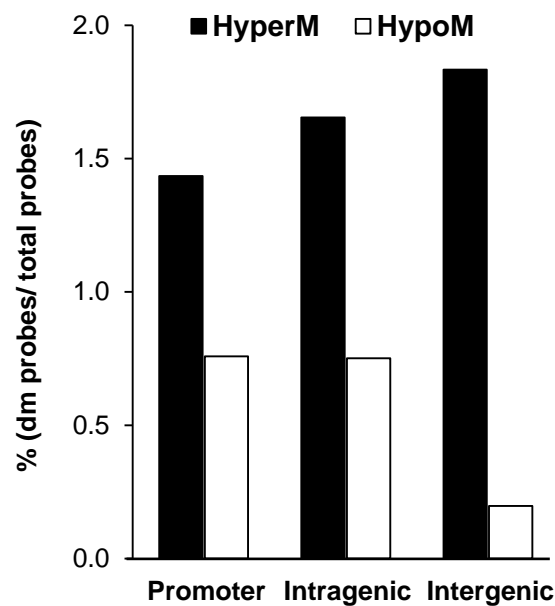
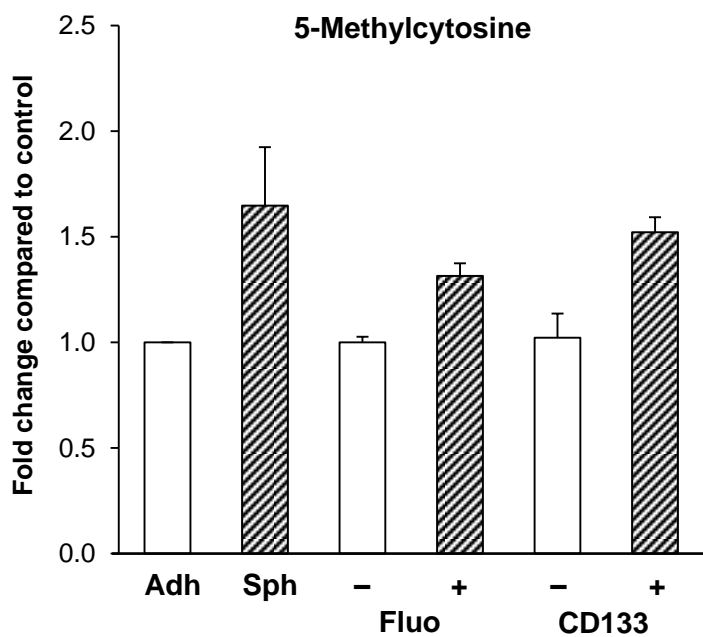
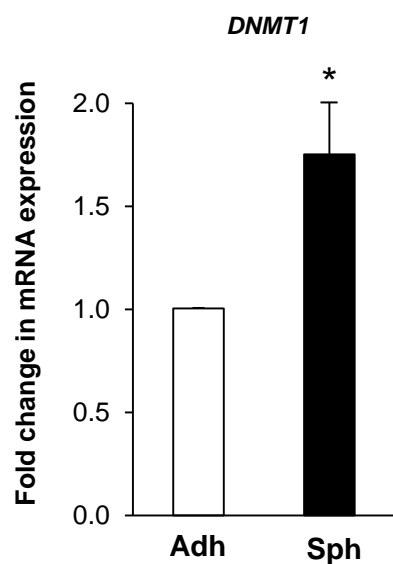
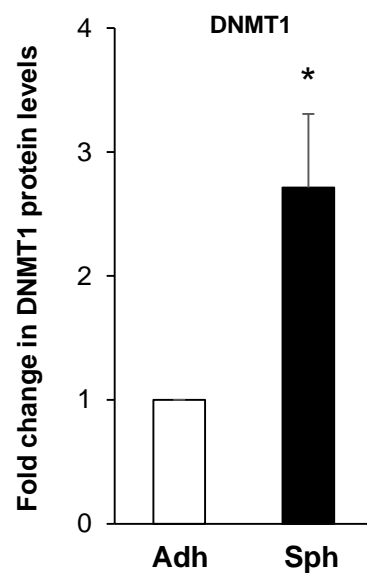
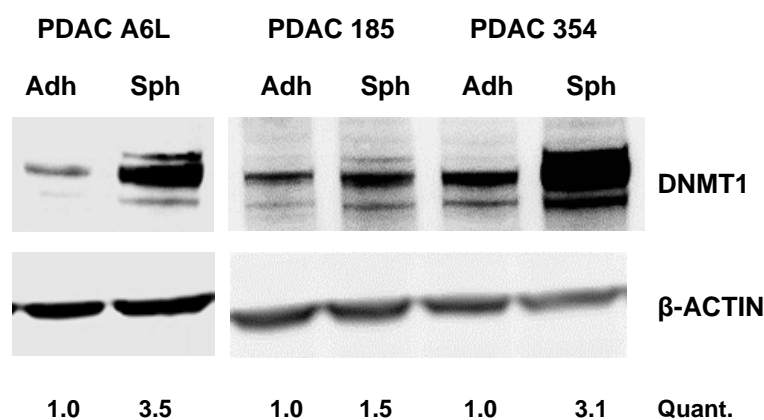


Figure 2 – Pancreatic CSCs overexpress DNMT1

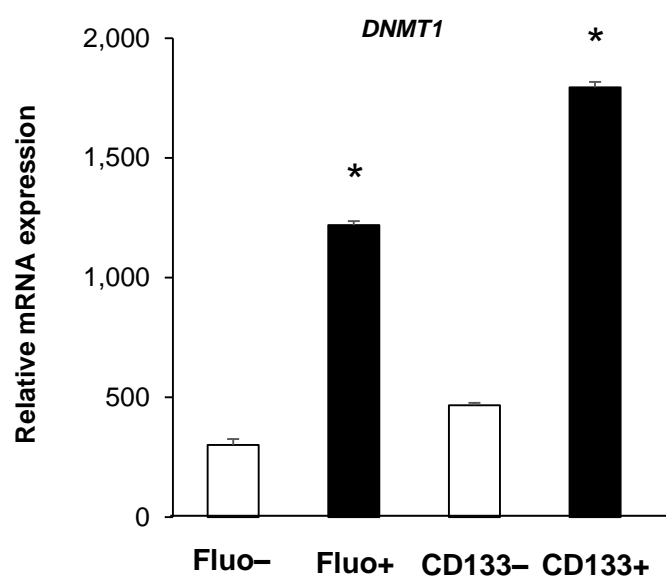
A



B



C



D

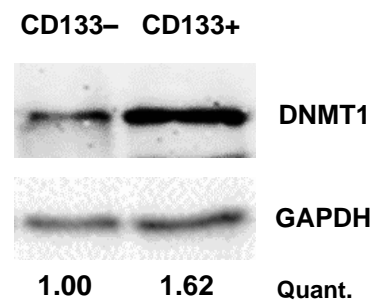


Figure 3 – DNMT1 inhibitor Zebularine decreases CSCs phenotypes

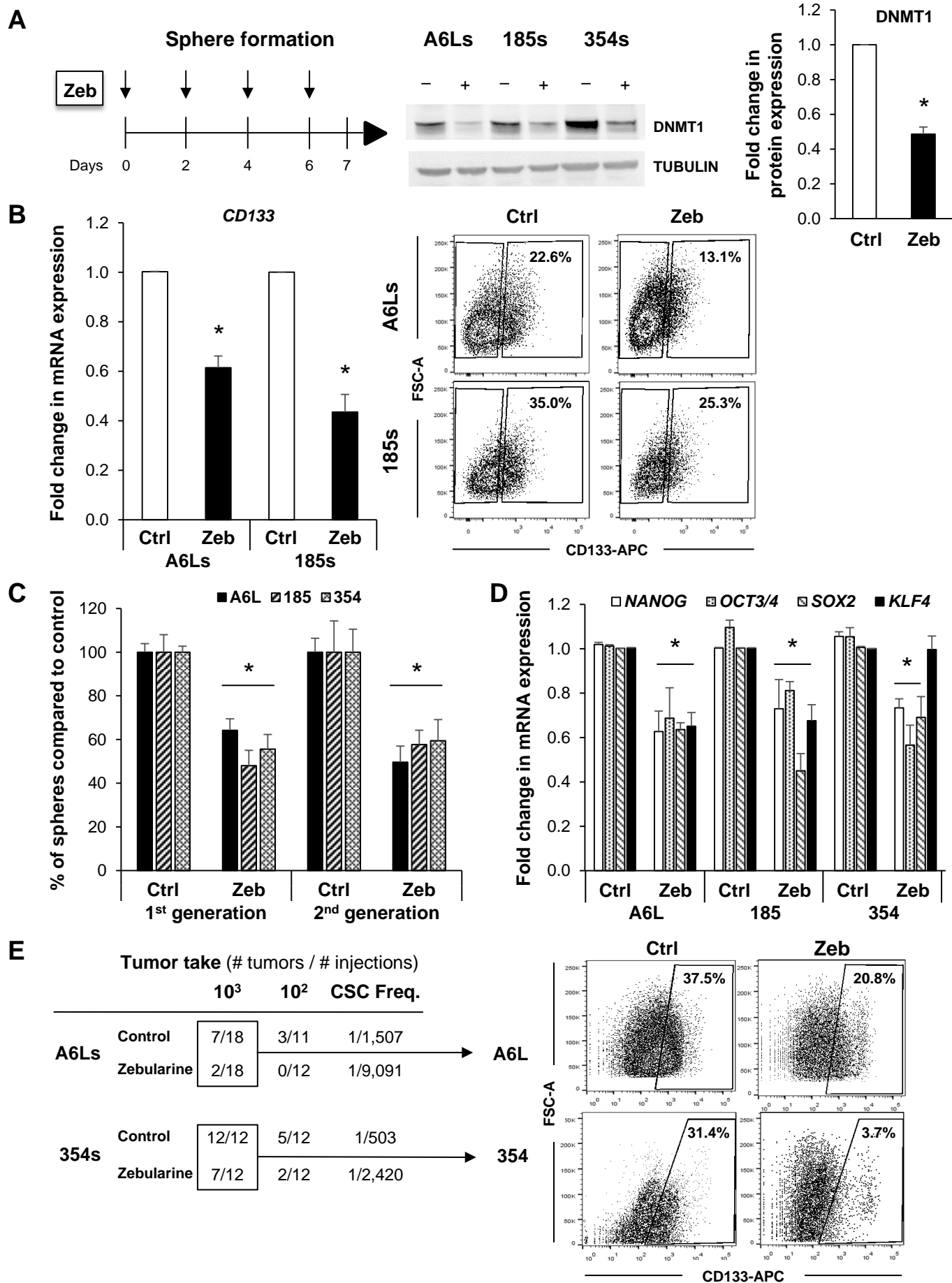


Figure 4 – Knockout of DNMT1 decreases CSCs phenotypes

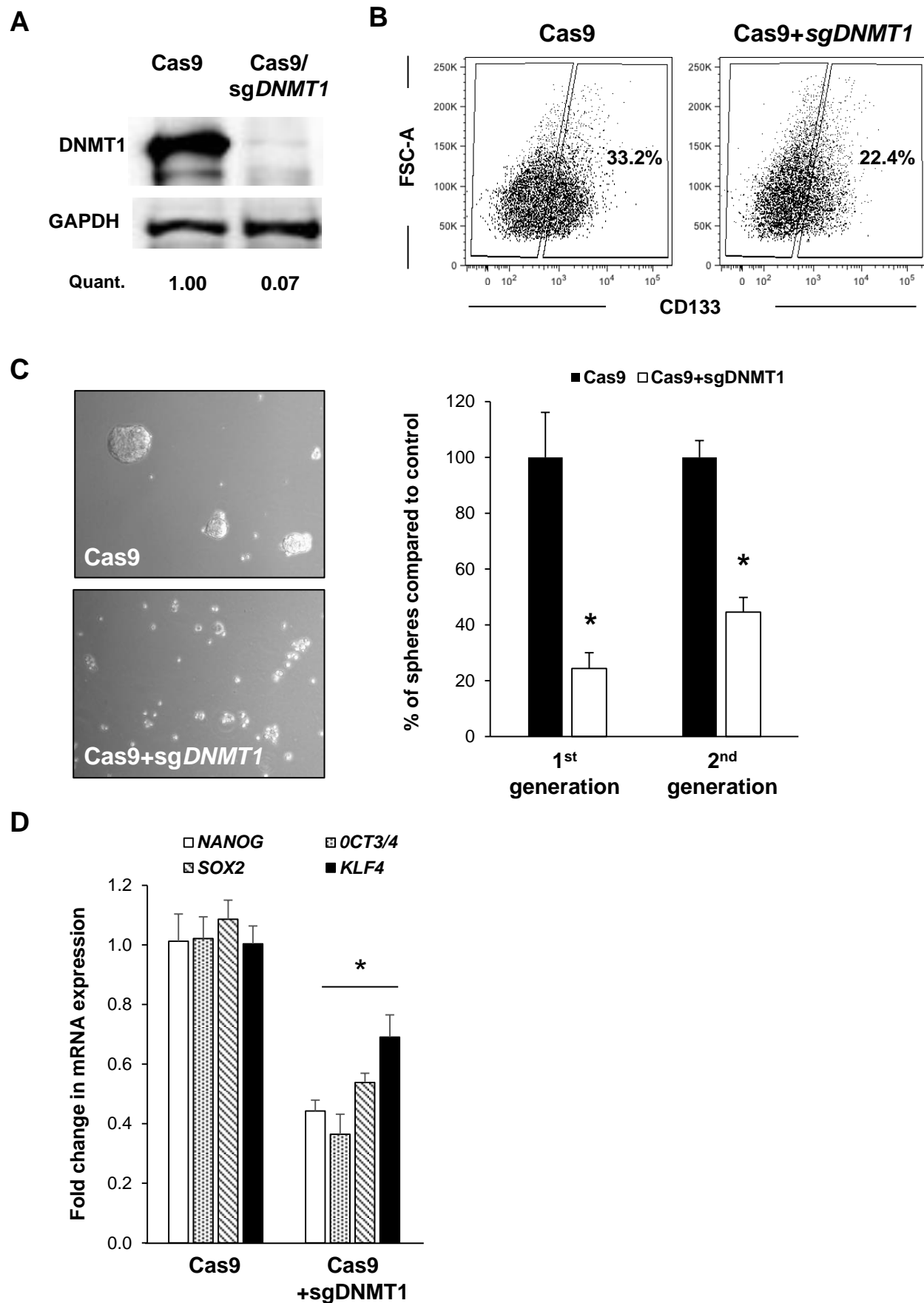


Figure 5 – Zebularine promotes CSC proliferation and differentiation

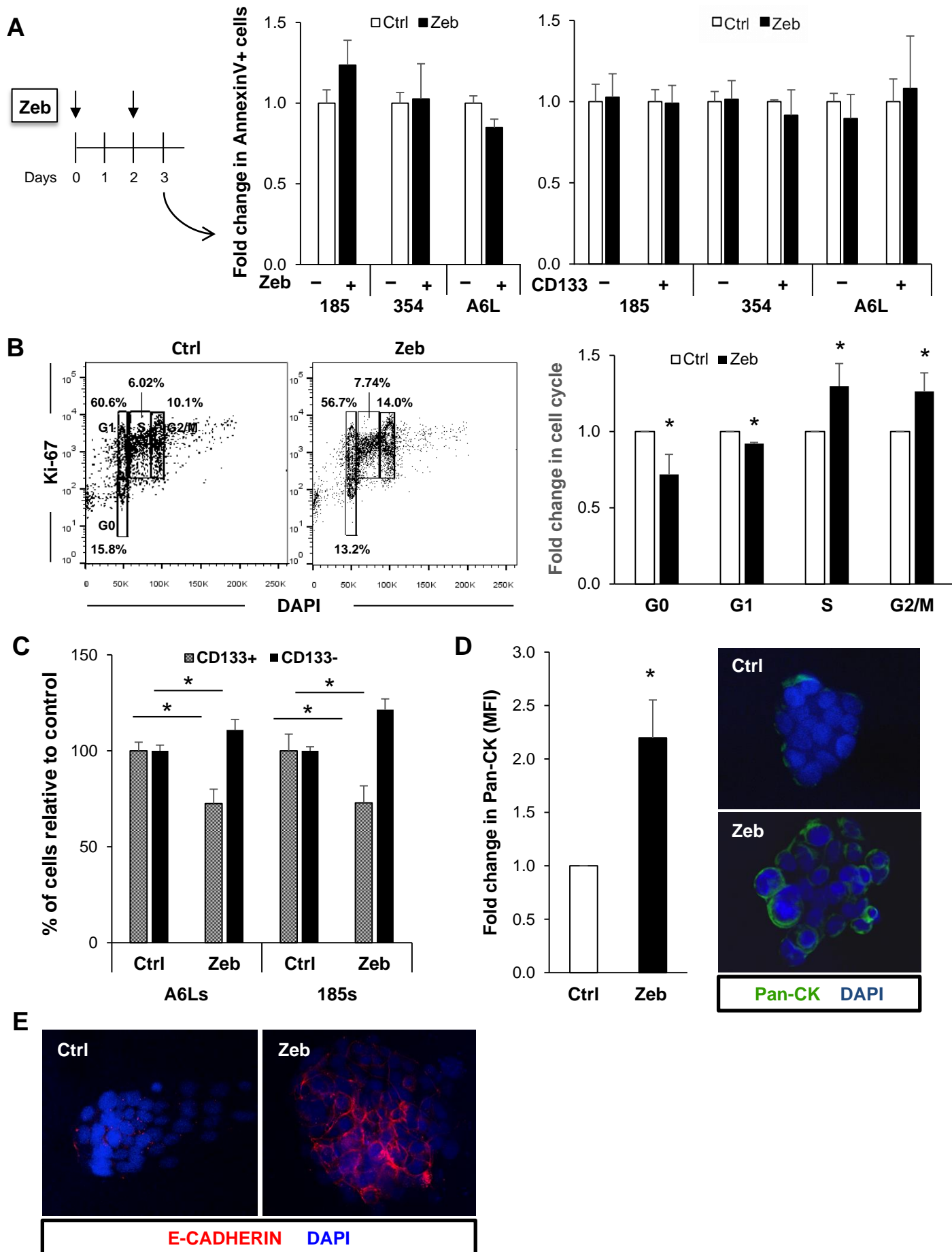


Figure 6 – Effect of Zebularine is mediated via hypomethylation of the miR-17-92 cluster

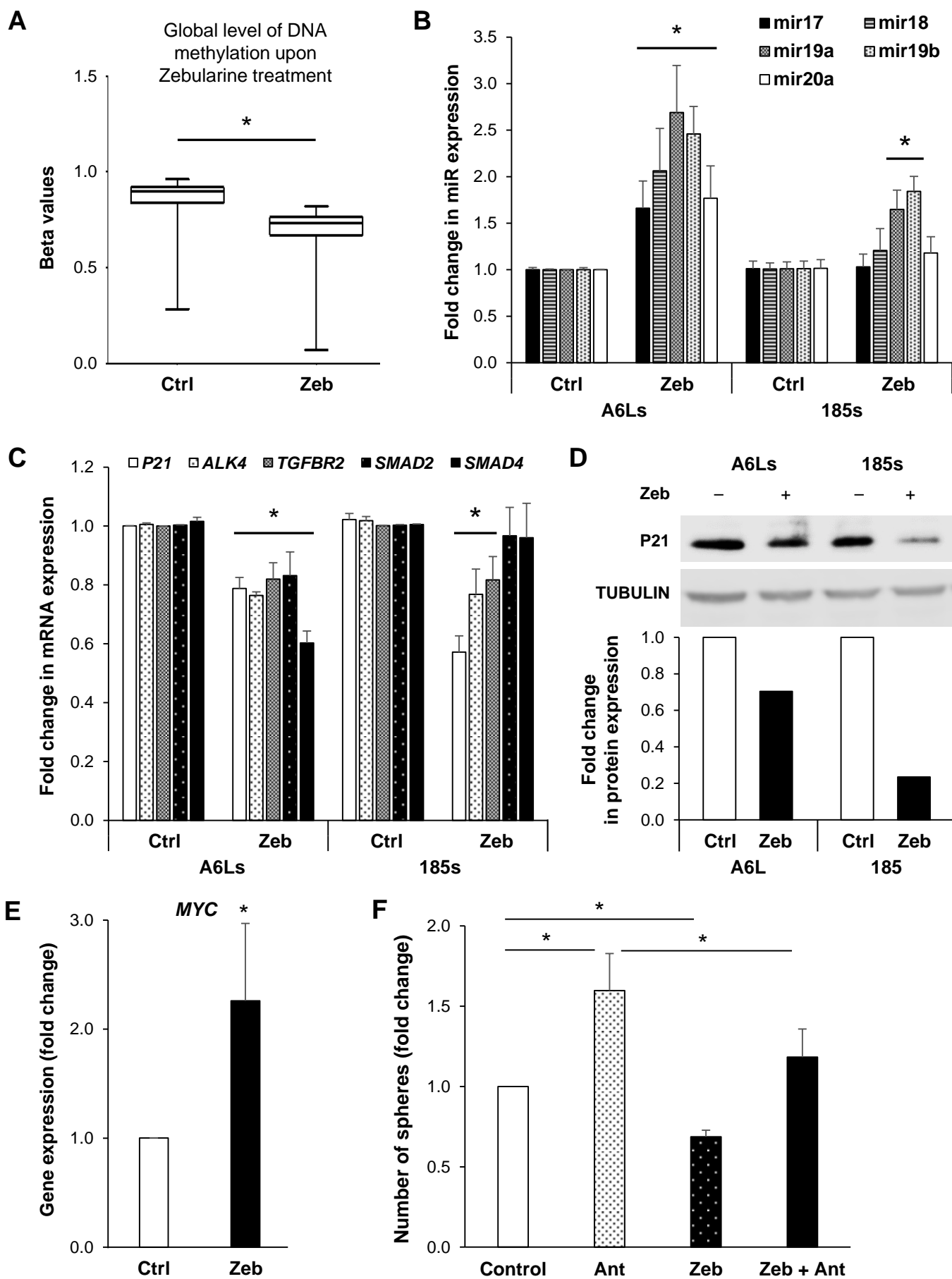


Figure S1 – Autofluorescence as a biomarker for pancreatic cancer stem cells

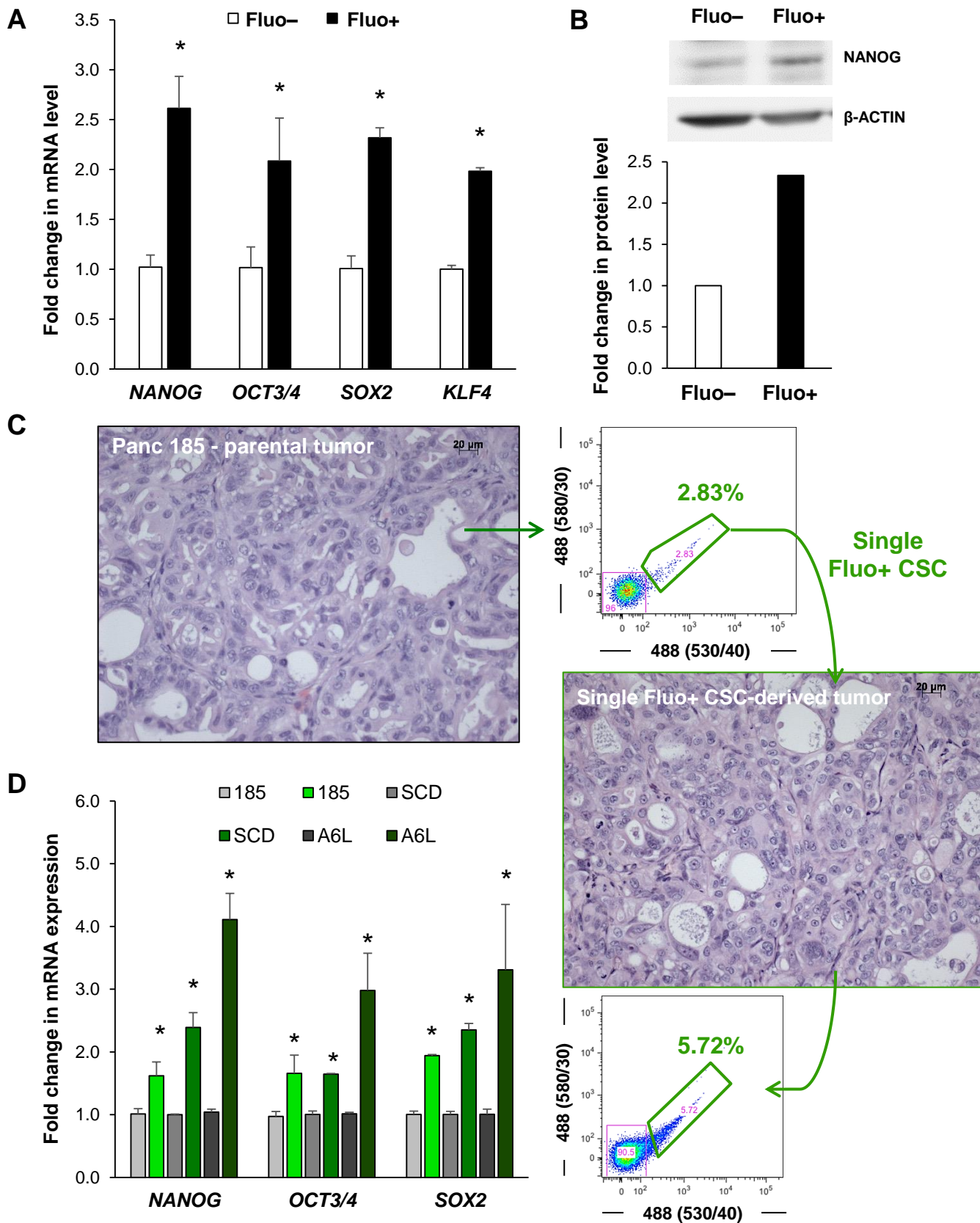


Figure S2 – PDAC CSCs over-express DNMT1 and bear higher 5mC levels

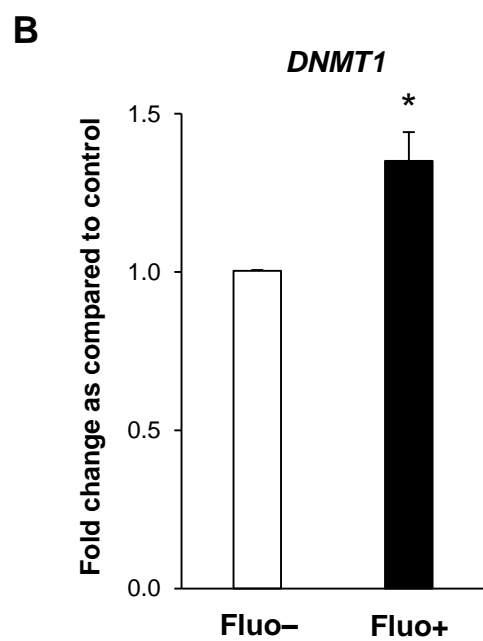
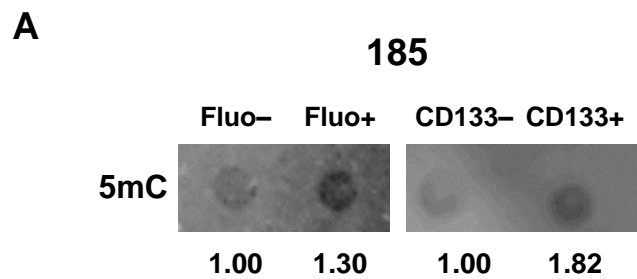


Figure S3 – DNMT1 inhibitor Zebularine decreases CSC phenotype

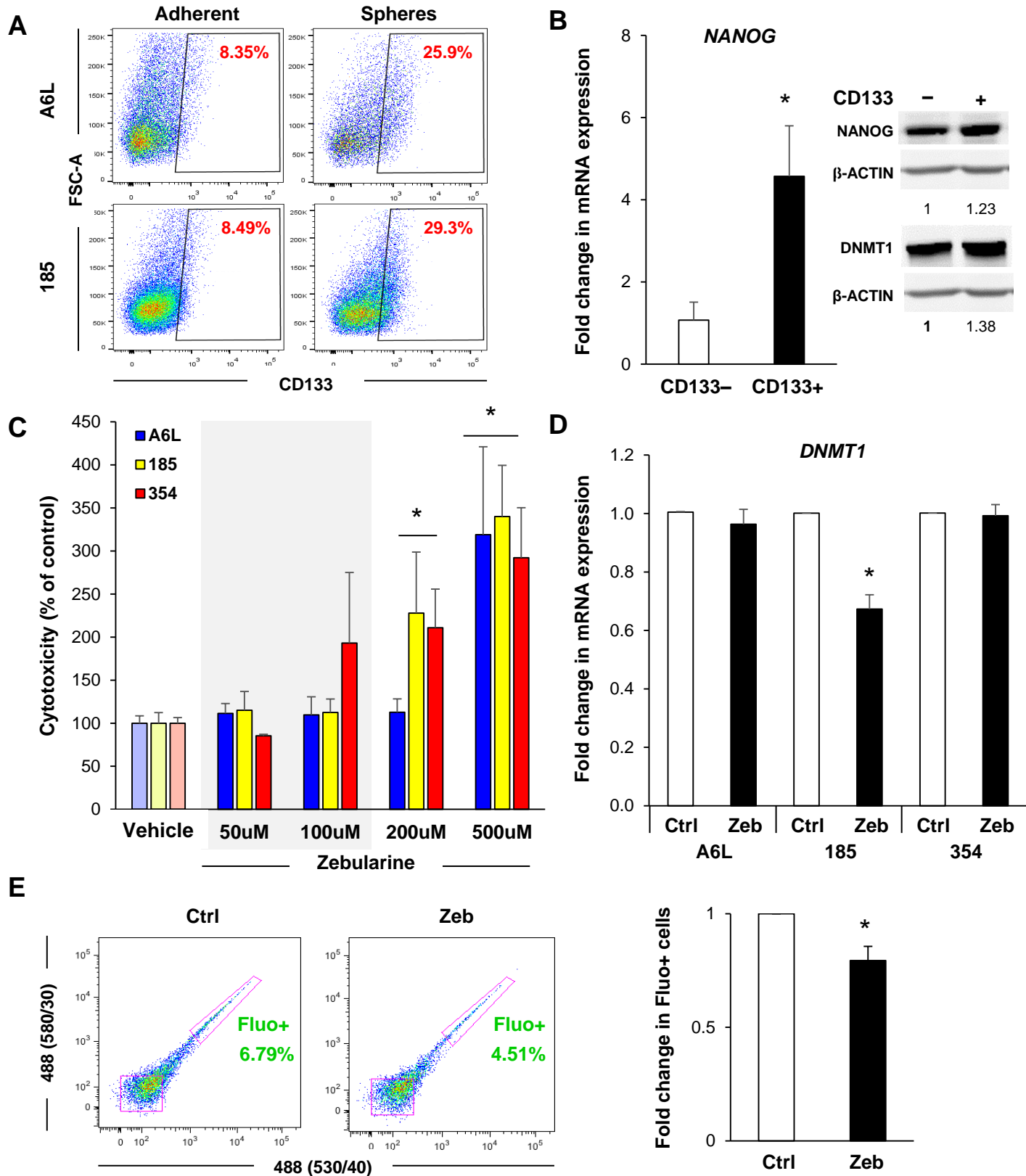


Figure S4 – DNMT1 inhibitor Decitabine decreased CSC phenotypes

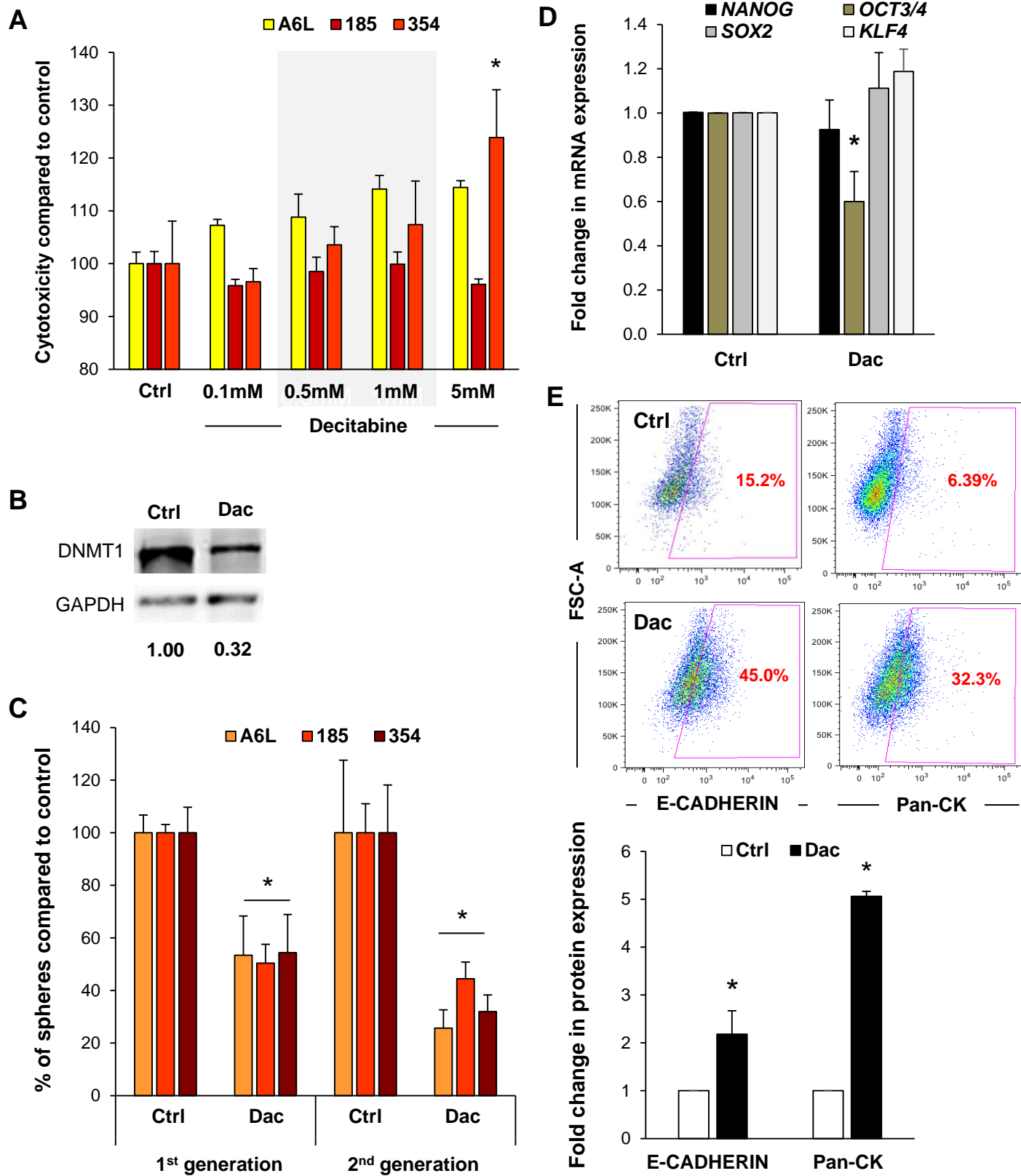
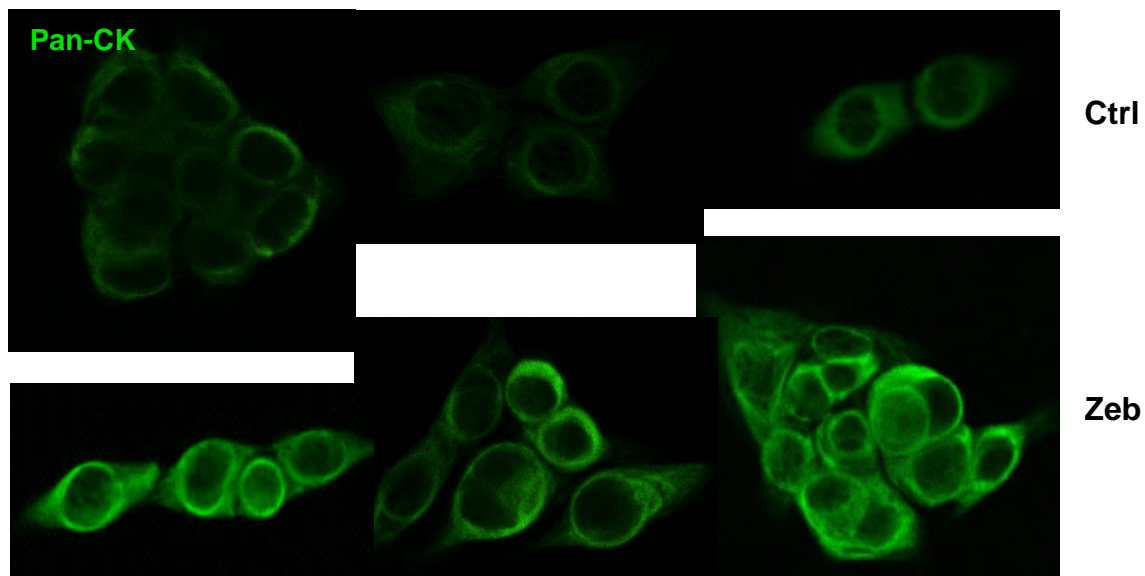
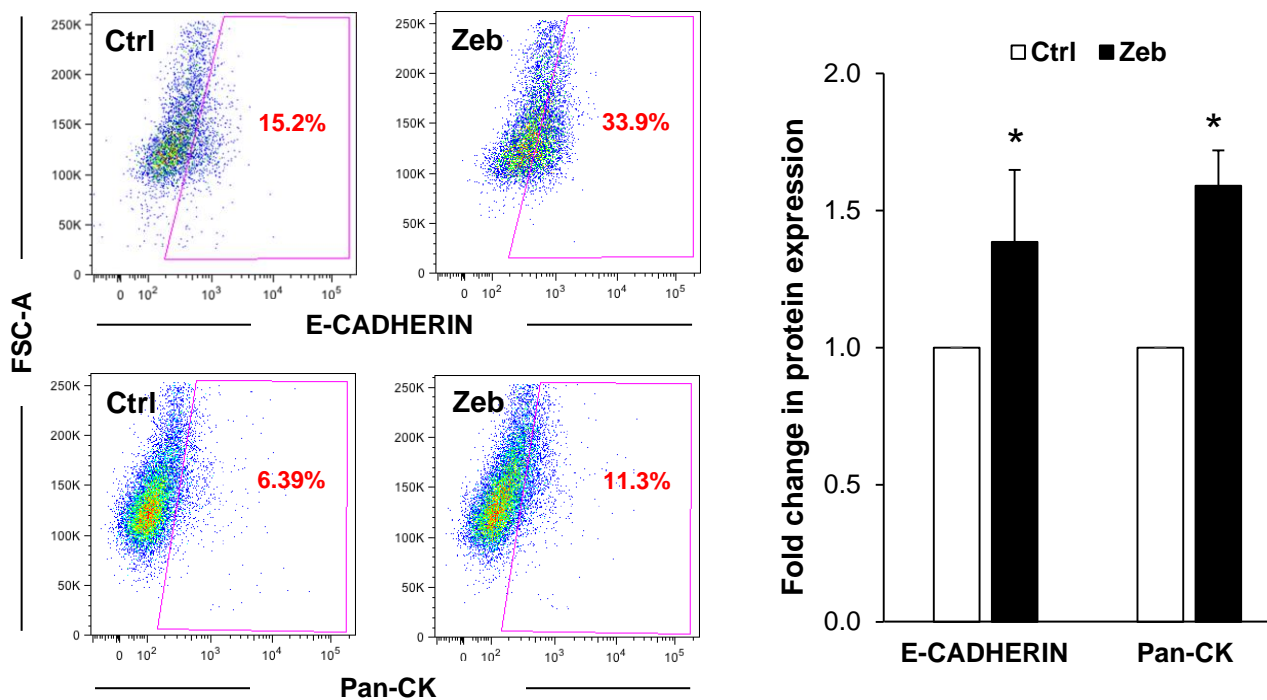


Figure S5 – DNMT1 inhibitor Zebularine promotes CSC differentiation

A



B



C

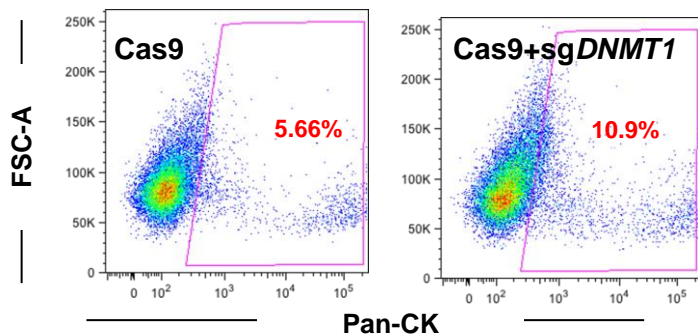


Figure S6 – DNMT1 inhibition modulates expression of miR-203, miR-205, and the miR-17-92 cluster

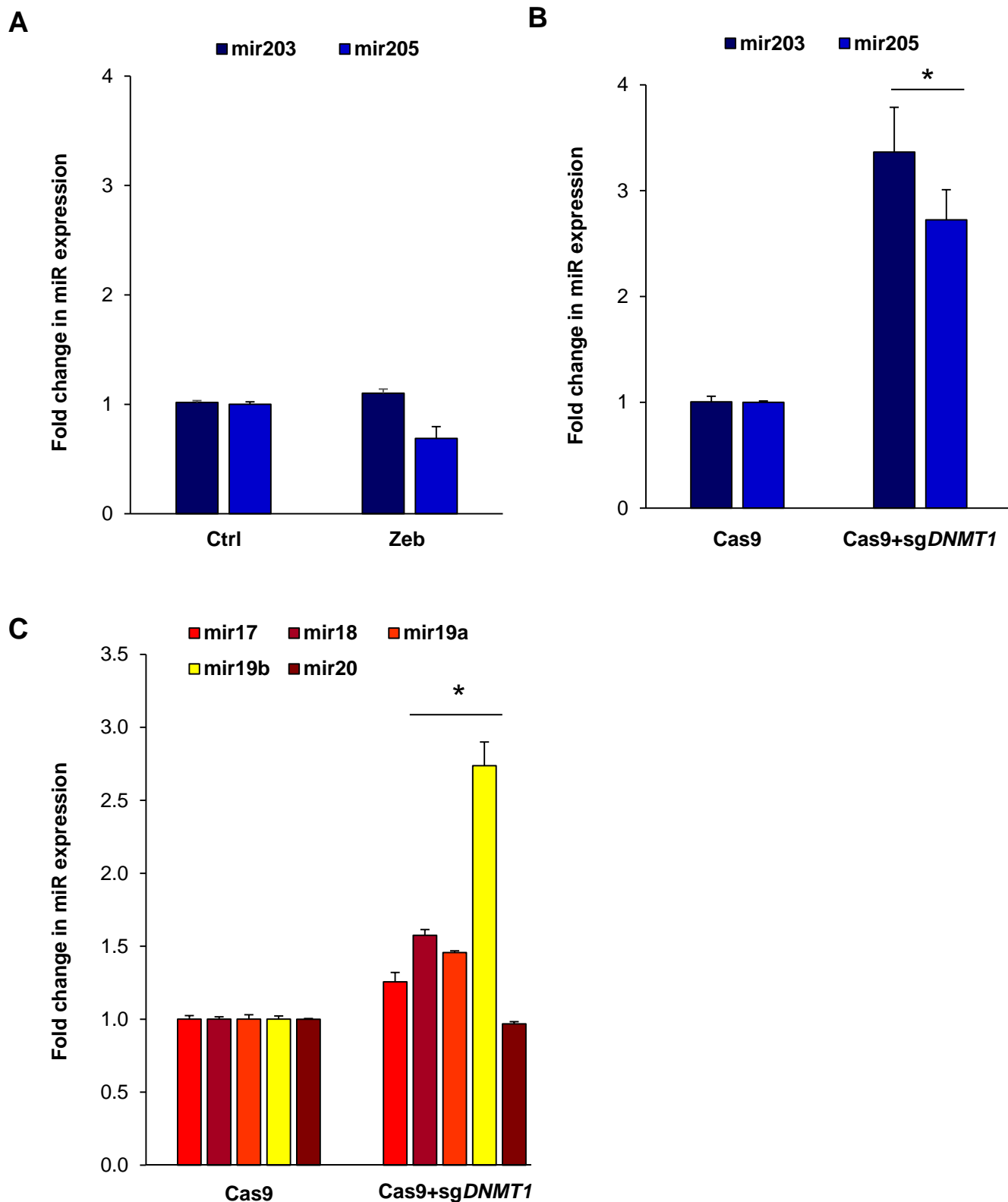


Table S1 – Decreased DNA methylation of genes upon Zebularine treatment

Gene_Name	FC_Zeb vs Ctrl	Gene_Name	FC_Zeb vs Ctrl
PRR3/GNL1	0.09	BCAR1	0.48
LIFR	0.23	ICT1	0.48
UBE2G1	0.27	RAB6A	0.48
KIAA1432	0.30	TCTE1	0.48
ITSN1/CRYZL1	0.30	MYADM	0.48
HIST1H4K	0.33	ELAC2	0.48
PITX1	0.34	EIF3I	0.48
HIST1H3I	0.34	ZNF784	0.48
HES2	0.34	DPP3	0.48
GARNL3	0.35	TRIM24	0.48
LOC389333	0.37	BCCIP	0.48
UXS1	0.37	PSTPIP2	0.48
LANCL1/CPS1	0.38	PRKAG2	0.48
PCBD2	0.38	LYST	0.48
SSTR5/LOC146336	0.39	DUSP1	0.48
PSTK	0.39	C1orf210	0.48
NDUFS6	0.40	CBR1	0.48
ADC	0.40	SIN3A	0.48
ZBTB7A	0.40	KIAA0802	0.49
HIST1H2AJ/HIST1H2BM	0.40	NDE1	0.49
FOXP1	0.40	C21orf96	0.49
EEF1A1	0.40	ALKBH5	0.49
HDHD2	0.40	FRAS1	0.49
USP1	0.41	ANKH	0.49
MAPKBP1	0.41	IFNGR1	0.49
ZFP36	0.42	ATP1A1	0.49
SGK3	0.42	KCNT1	0.49
TUBB2B	0.42	CDC6	0.49
GCLC	0.43	LEPR/LEPROT	0.49
SOX2OT/SOX2	0.43	SLC7A6	0.49
SHOX2	0.43	EZH2	0.49
UBAC2	0.43	DCP1A	0.49
ILF3/LOC147727	0.43	HNRNPD	0.49
STX5	0.44	C2orf63/RPS27A	0.49
HLA-DRB1	0.44	PCDHGA1	0.49
SPEN/FLJ37453	0.44	GPX5	0.49
SGEF	0.44	BAT2L2	0.50
ECHDC2	0.44	HIST2H2AA3	0.50
HIST1H4J	0.45	FAM119A	0.50
MAP6D1	0.45	MTCH1	0.50
LOC100130987/RAD9A	0.45	FDX1L	0.50
VPRBP	0.46	TNPO3	0.50
TMEM179B/TAF6L	0.46	C7orf55	0.50
DOCK1	0.46	AS3MT	0.50
PTGER3	0.46	UNC84A	0.50
EFHC1	0.46		
ANKRD57	0.46		
TMEM108	0.46		
HIST1H4J	0.47		
ERICH1	0.47		
PLEK2	0.47		

Table S2 – Increased DNA methylation of genes upon Zebularine treatment

Gene_Name	FC_Zeb vs Ctrl	Gene_Name	FC_Zeb vs Ctrl
LRP11	9.51	DCUN1D4	2.51
HOXA3	9.20	PCDHB10	2.51
CMTM3	7.71	APP	2.50
TRMT11	7.27	ALDH1A3	2.50
SFRS2IP	5.99	MIR548I4/CNTNAP2	2.49
LYN	5.06	MEF2D	2.49
EXOC4	3.72	TRIM25	2.48
TESK2	3.65	IFNAR2	2.47
RNF168	3.59	KLC4/MRPL2	2.47
SIVA1	3.54	CLUL1	2.47
FKBP2	3.42	DTL	2.46
TMEM160	3.17	MAP3K5	2.46
LPHN2	2.85	OXCT1	2.45
METT10D	2.85	HIST1H4E	2.45
CHD9	2.84	FDFT1	2.45
RAD51	2.84	TMED10	2.45
ESYT1	2.76	UGDH	2.45
NFYA/C6orf130	2.74	PJA2	2.43
H2AFY2	2.73	EIF3H	2.43
NAV1	2.72	PSMC2	2.43
BLZF1/NME7	2.71	SOCS4/WDHD1	2.43
C6orf192	2.70	OR5I1	2.43
KCTD6	2.70	ELL2	2.42
SYCP3	2.69	GRB2	2.42
UTRN	2.69	FUK	2.42
NEDD9	2.68	ATP5J/GABPA	2.41
FTO/RPGRIP1L	2.68	HIST1H2BM/HIST1H2AJ	2.41
BAI2	2.68	BAT4/CSNK2B	2.41
ZNF518A	2.67	SOX2OT/SOX2	2.40
BRCA2	2.66	CTNND1	2.40
MAPKAP1	2.65	SYDE2	2.40
SNORD50A/SNHG5	2.64	SFRS12IP1	2.40
ATN1	2.63	NMI	2.40
TPM3	2.63	NCRNA00120/AKIRIN2	2.39
KCTD11/ACAP1	2.63	GRB2	2.39
MAP7	2.62	PROX1	2.39
SF3B1	2.62	USP13	2.39
SLC35A1	2.61	BAI3	2.39
ANO4	2.61	RBM47	2.39
DAXX	2.61	GLI1	2.38
KIF11	2.60	RAP2A	2.38
ZNF613	2.60	RPLP2	2.38
NCOA6	2.58	NAA16	2.38
ABCF1	2.58	CDC14B	2.37
MACC1	2.58	MYO16	2.37
SNHG3-RCC1	2.57	PTP4A2	2.37
ZDHHC20	2.56	BET1	2.37
C18orf54	2.56	C1orf25	2.37
WHSC1L1	2.55	SYNE2	2.37
HIST2H2AA4/HIST2H2AA3	2.55	FLJ45244/DICER1	2.36
RFC3	2.55	HOXC11	2.36
DAPK3	2.55	HSPC072/LOC100270804	2.35
RB1CC1	2.53	PSMA1	2.35
LARS2	2.52	GTF3A	2.35

Table S2 – Increased DNA methylation of genes upon Zebularine treatment

Gene_Name	FC_Zeb vs Ctrl	Gene_Name	FC_Zeb vs Ctrl
RNASEK	2.35	RPL7/RDH10	2.26
C10orf53	2.35	C5orf44/TRIM23	2.26
CD2AP	2.35	IMPAD1	2.25
PSMG2/CEP76	2.34	HARS	2.25
KIAA1244	2.34	SLC25A13	2.25
DCP2	2.34	CARD6	2.25
CNN3	2.34	KIAA0146	2.25
BZW2/ANKMY2	2.33	PES1	2.24
DLAT	2.33	ZMYND11	2.24
SLC7A11	2.33	GTPBP8	2.24
BTN2A1	2.33	HARBI1/KIAA0652	2.24
RAD54B	2.33	C12orf11/FGFR1OP2	2.24
C6orf165	2.33	UBR5	2.23
CYBASC3/TMEM138	2.33	S100A10	2.23
GNAO1	2.32	TMEM49/PTRH2	2.23
MRPS30	2.32	VWC2	2.23
SIN3A	2.32	FSIP1	2.23
SLC2A1	2.32	MRPS28	2.22
ZNF259	2.32	HAX1	2.22
HIST1H2AC/HIST1H2BC	2.31	LRRK1	2.22
B3GALT1	2.31	CASC5	2.22
RPL14	2.31	BRIX1/RAD1	2.22
API5	2.31	C7orf36	2.22
TMEM87A	2.30	ALK	2.22
MCM4	2.30	ZDHHC5	2.21
NDC80/METTL4	2.30	ADAR	2.21
ATF6B	2.30	LENG9	2.21
PTPRD	2.30	NR1H3/ACP2	2.21
MAP4K1/EIF3K	2.30	LARP7/C4orf21	2.21
BRE/RBKS/LOC100302650	2.30	MAP4	2.21
MTRF1L	2.29	PHF12	2.21
SC4MOL	2.29	IPMK	2.21
TOLLIP	2.29	VPS25	2.21
LAMB2	2.29	C2orf60	2.20
NT5DC3	2.29	NFIL3	2.20
CBR4	2.29	KIAA0319L	2.20
PRLR	2.29	TBC1D4	2.20
ARL5A	2.29	CBARA1	2.20
PLK1	2.28	MAGI1	2.20
IWS1	2.28	TP53BP1	2.19
SLC12A9	2.28	MIPOL1	2.19
HNRNPC	2.28	SLC1A3	2.19
NRP1	2.28	C17orf80/FAM104A	2.19
NMT1/DCAKD	2.28	MADD	2.19
IL17RD	2.27	HIST1H1E	2.18
DAB2	2.27	ALG14	2.18
LOC552889	2.27	SACM1L	2.18
UFD1L/CDC45L	2.27	MRFAP1L1	2.18
CDK6	2.27	ALCAM	2.18
TSNAX-DISC1	2.26	MED7	2.18
SEPHS2	2.26	DTWD2	2.18
TMED7-TICAM2	2.26	DLG2	2.18
KRT10/TMEM99	2.26	SLC25A36	2.18
RNF111	2.26	ZNF773	2.17

Table S2 – Increased DNA methylation of genes upon Zebularine treatment

Gene_Name	FC_Zeb vs Ctrl	Gene_Name	FC_Zeb vs Ctrl
RAI14	2.17	C6orf52/PAK1IP1	2.13
BRD2	2.17	ETAA1	2.13
C14orf106	2.17	HSD11B1L/C19orf70	2.13
KLF9	2.17	ATF2/MIR933	2.13
C11orf65	2.17	DLGAP5	2.13
NUP98	2.17	HIVEP3	2.13
MRPS12/SARS2	2.17	ALG14	2.13
NUF2	2.17	HERC4	2.12
CHD3	2.17	MRPS33	2.12
RRM2B	2.17	C21orf54	2.12
COX7A2	2.17	TNFRSF11A	2.12
SERPINI1/PDCD10	2.16	C16orf46	2.12
MED27	2.16	RPL22	2.12
C16orf71/ANKS3	2.16	MRPS14	2.12
UFD1L/CDC45L	2.16	C10orf131	2.12
BTAF1	2.16	HFE	2.12
LHFP	2.16	ADPRHL2	2.12
ZRANB2	2.16	PSPC1	2.12
TRIM26	2.16	ARGLU1	2.11
POLR1A	2.16	RAB12	2.11
AGPAT1/RNF5/RNF5P1	2.16	CAPZA1	2.11
CCDC94	2.16	MRPS33	2.11
ZBTB9	2.16	LRCH3	2.11
DERL2/MIS12	2.15	TMTC2	2.11
MIR548G/C3orf26	2.15	LOC285830	2.11
ERGIC2	2.15	THNSL1/ENKUR	2.11
LOC100216545	2.15	TMTC2	2.11
ATF4	2.15	HIST1H2AB	2.11
SKA3/MRP63	2.15	VTI1A/ZDHHC6	2.11
ARID2	2.15	USP39	2.11
ANKRD34A/POLR3GL	2.15	FAM109A	2.11
DEFA5	2.15	TLE4	2.11
MAT2B	2.15	TSN	2.11
ZNF687	2.15	ROBO3	2.11
CWC22	2.14	C10orf114	2.10
MALAT1	2.14	SV2C	2.10
C4orf33	2.14	NECAB1	2.10
LOC100190939/TPT1	2.14	TFIP11	2.10
LIPH	2.14	DCBLD2	2.10
EIF3B	2.14	IPO11	2.10
MLX	2.14	ZNF219/C14orf176	2.10
TMCO6	2.14	PRIM2	2.10
SPATA17/GPATCH2	2.14	HNF1A	2.10
PNPLA3	2.14	C13orf38	2.10
C12orf76	2.14	C12orf72	2.10
BAT3	2.13	FLJ43663	2.10
RPS27	2.13	MLH1/EPM2AIP1	2.10
KDM1A	2.13	MRPS36	2.10
PLEKHM1	2.13	HSBP1L1	2.10
FBXW8	2.13	ANKFY1	2.10
SDAD1	2.13	NCEH1	2.10
PGAP2/NUP98	2.13	PAPOLG	2.09
PSMB8	2.13	LMBR1	2.09
SRPK1	2.13	ZNF423	2.09

Table S2 – Increased DNA methylation of genes upon Zebularine treatment

Gene_Name	FC_Zeb vs Ctrl	Gene_Name	FC_Zeb vs Ctrl
WDR89	2.09	ATP13A3	2.07
HIST1H1D	2.09	VPS45	2.07
RPS11	2.09	KIAA0907	2.07
SP2	2.09	SETD2	2.07
SNW1/C14orf178	2.09	ORC1L/PRPF38A	2.07
KIAA0319	2.09	BNIP1	2.07
EHBP1	2.09	SFRS13A	2.07
ZBTB4/POLR2A	2.09	OSBP	2.07
TMEM68/TGS1	2.09	MPZL2	2.07
IMMT	2.09	WDR46/PFDN6	2.07
HM13	2.09	KIAA0427	2.07
TMF1	2.09	ZFYVE26	2.07
INSIG2	2.09	HIST1H2AC	2.07
OSTC	2.09	OGG1	2.07
LPHN1	2.09	HELQ/MRPS18C	2.07
PPP2R3C/KIAA0391	2.09	MXI1	2.07
PODNL1/DCAF15	2.09	SYF2	2.07
C7orf64/PEX1	2.09	TOMM7	2.07
LSR	2.09	PTEN/KILLIN	2.07
ZNF184	2.09	RNGTT	2.07
VEZF1	2.09	NPC2	2.07
ZNF705A/FAM66C	2.09	CENPO	2.07
ACCN1	2.09	KRAS	2.06
DLX2	2.09	RPUSD2	2.06
CHD7	2.09	RGS2	2.06
ANO4	2.09	SORL1	2.06
ABCF1	2.09	LOC388789	2.06
UNC45A	2.08	C1orf204	2.06
ELP3	2.08	C4orf3	2.06
ZNF440	2.08	RPL24	2.06
CEP164	2.08	UBXN2A	2.06
KAT2B	2.08	PRKG1	2.06
CYB5A	2.08	MRPS36	2.06
CDV3	2.08	SETD5	2.06
NME7/BLZF1	2.08	MEPCE/ZCWPW1	2.06
FKBP1	2.08	CA8	2.06
PRNP	2.08	RPL7	2.06
ZNF426	2.08	ITGAV	2.06
SLK	2.08	MET	2.06
KCTD21/USP35	2.08	FCF1/KIAA0317	2.06
EHMT2	2.08	DDX18	2.06
APOC1	2.08	DPYD	2.06
SAPS2	2.07	VTI1B	2.06
TPI1	2.07	CD8A	2.06
ASNSD1	2.07	SLC39A7/RXRB	2.05
TMEM143/SYNGR4	2.07	RPS6KC1	2.05
KLF9	2.07	SMARCA1	2.05
C2orf60	2.07	HOXA3	2.05
CASC2/RAB11FIP2	2.07	CTDSPL2	2.05
AHCYL1	2.07	KCTD18	2.05
C13orf23/NHLRC3	2.07	HIST1H2BN	2.05
ZNF192	2.07	CCND3	2.05
AGPAT1/RNF5/RNF5		SCARNA16/C17orf86	2.05
P1	2.07	RSL1D1	2.05
CHURC1	2.07		

Table S2 – Increased DNA methylation of genes upon Zebularine treatment

Gene_Name	FC_Zeb vs Ctrl	Gene_Name	FC_Zeb vs Ctrl	Gene_Name	FC_Zeb vs Ctrl
BCO2	2.05	KBTBD5	2.02		
C1orf31	2.05	C10orf140	2.02	NQO1	2.00
RUNX1	2.05	BDP1	2.02	ALS2CR4	2.00
CD55	2.05	LANCL1/CPS1	2.02	ANKRD10	2.00
KIAA1522	2.05	DPYSL2	2.02	MTFMT	2.00
TIMELESS	2.05	HIP1	2.02	MED17	2.00
CCDC18/TMED5	2.05	ZADH2/TSHZ1	2.02	ARMC8	2.00
ATOX1	2.04	ROBO1	2.02	MTX2	2.00
TACO1	2.04	FBXW8	2.02	ANGEL2	2.00
NAPB	2.04	UBR4	2.02		
PEX7	2.04	IFI16	2.02		
C4orf32	2.04	BTBD9	2.02		
NCRNA00081/SHOC2	2.04	ACAD11	2.02		
WBP4	2.04	DTNBP1	2.02		
TUFM	2.04	PCDH7	2.02		
TRIM27	2.04	ZFP36L2/LOC100129726	2.02		
IRF2BP2	2.04	PEX13	2.02		
RTTN	2.04	MAF	2.02		
HNRNPA1/CBX5	2.04	HIST1H2AG/HIST1H2BJ	2.02		
EIF3E	2.04	RASL11B	2.02		
MOBK1A	2.04	ORC6L/VPS35	2.02		
ERCC5	2.04	RAB13	2.01		
CRAMP1L	2.04	SLK	2.01		
ATP5G1	2.04	SPRY1	2.01		
RBPJL/MATN4	2.04	CCDC49	2.01		
PFDN6/WDR46	2.04	CCDC21	2.01		
GLCCI1	2.04	CCDC14	2.01		
S100A11	2.03	FBXL3	2.01		
FAM102B	2.03	KLHDC4	2.01		
SFPQ	2.03	TRIM45	2.01		
HIST1H2AB	2.03	TBP	2.01		
SNORA7A/RPL32	2.03	AICDA	2.01		
HNRNPM	2.03	RFXANK	2.01		
SLC35E3	2.03	NUP188/	2.01		
ANKRD11	2.03	FBXO16	2.01		
BUB1	2.03	UBP1	2.01		
OR1E2	2.03	GNAI3	2.01		
ASAH1	2.03	A2BP1	2.01		
DARS	2.03	AASDH	2.01		
CTDSP2	2.03	GPM6A	2.01		
PTTG1IP	2.03	UBN2	2.01		
TMX4	2.03	PIK3R3	2.01		
ANAPC7	2.03	TAF11/ANKS1A	2.01		
YARS	2.03	LSG1	2.01		
RND3	2.03	TMEM67	2.01		
GBX1	2.03	MSH5	2.01		
OSGEPL1	2.02	NPM1	2.01		
CACNA2D3	2.02	C9orf130	2.00		
BAD/GPR137	2.02	RPL32P3	2.00		
NRD1	2.02	SCGB2A2	2.00		
TRIM2	2.02	YWHAG	2.00		
TRPM5	2.02	CDC42EP3	2.00		
MACF1	2.02	C19orf35	2.00		
NUAK2	2.02	EXOSC9	2.00		

Table S3 – Decreased DNA methylation for miRs following Zebularine treatment

hsa-miRNA	FC_Zeb vs. Ctrl
hsa-miR1470	0.61
hsa-miR548G	0.61
hsa-miR548G	0.69
hsa-miR205	0.71
hsa-miR1470	0.73
hsa-miR205	0.73
hsa-miR1470	0.74
hsa-miR548N	0.77
hsa-miR548N	0.78
hsa-miR205	0.78
hsa-miR548N	0.78
hsa-miR548G	0.80
hsa-miR1236	0.58
hsa-miR548H4	0.62
hsa-miR636	0.62
hsa-miR203	0.69
hsa-miR26B	0.70
hsa-miR1236	0.70
hsa-miR636	0.72
hsa-miR423	0.75
hsa-miR219-1	0.76
hsa-miR148A	0.77
hsa-miR26B	0.78
hsa-miR423	0.78
hsa-miR148A	0.78
hsa-miR219-1	0.79
hsa-miR548H4	0.79
hsa-miR203	0.80
hsa-miR760	0.61
hsa-miR1915	0.62
hsa-miR1324	0.63
hsa-miR2277	0.67
hsa- miR15B /miR16-2	0.68
hsa-miR548F1	0.69
hsa-miR2110	0.70
hsa-miR346	0.70
hsa-miR92B	0.71
hsa-miR654/miR376B/miR376A2/miR300/miR376A1	0.71
hsa-miR1292	0.72
hsa-miR1322	0.72
hsa-miR1539	0.72
hsa-miR611	0.72
hsa-miR129-1	0.72
hsa-miR564	0.73
hsa-miR132/miR212	0.73
hsa-miR1205	0.73
hsa-miR301B/ miR130B	0.74
hsa-miR548H3	0.74
hsa-miR600	0.74
hsa-miR27A/miR24-2/miR23A	0.75

Table S3 – Decreased DNA methylation for miRs following Zebularine treatment

hsa-miRNA	FC_ Zeb vs. Ctrl
hsa-miR202	0.75
hsa-miR570	0.75
hsa-miR567	0.75
hsa-miR585	0.76
hsa-miR592	0.76
hsa-miR375	0.76
hsa-miR339	0.77
hsa-miR191/miR425	0.77
hsa-miR150	0.77
hsa-miR130A	0.77
hsa-miR17HG	0.78
hsa-miR658	0.78
hsa-miR149	0.78
hsa-miR661	0.78
hsa-miR548K	0.78
hsa-miR1304	0.78
hsa-miR574	0.78
hsa-miR320A	0.79
hsa-miR16-2	0.79
hsa-miR30D	0.79
hsa-miR1977	0.79
hsa-miR190B	0.79
hsa-miR638	0.79
hsa-miR425	0.79
hsa-miR758/miR1197/miR329-1/miR323	0.79
hsa-miR596	0.79
hsa-miR451/miR144	0.79
hsa-miR10A	0.80
hsa-miR639	0.80
hsa-miR1252	0.80
hsa-miR10B	0.80
hsa-miR762	0.80
hsa-miR1287	0.80
hsa-miR141/miR200C	0.80
hsa-miR26A2	0.80

Given is the Fold Change (FC) of β -methylation values for Zebularine (Zeb) treatment vs control (ctrl). Only data for $FC \leq 0.80$ are provided.

Due to the presence of different probes targeting the same miRNAs, some are shown more than once.

SUPPLEMENTARY FIGURE LEGENDS

Supplementary Figure 1 – Autofluorescence as a biomarker for pancreatic cells stem cells.

(A) mRNA levels for pluripotency-associated genes in Fluo+ vs Fluo– sorted cells; PDAC-185 and -A6L, n=6, * p<0.05. **(B)** Nanog protein expression in Fluo+ and Fluo– cells. Representative Western blot using β -ACTIN as loading control. **(C)** H&E histology of the PDAC-185 parental tumor (upper left). Representative FACS plot for sorting of single Fluo+ cells (upper right). Arising tumors following injection of single cells into immunocompromised mice were digested and sorted for Fluo+ and Fluo– cells. Representative FACS plot is shown (lower right). **(D)** mRNA levels for pluripotency-associated genes for the parental 185 tumor, the single Fluo+ cell-derived tumor, and for A6L tumors are shown. * p<0.05, n=3 (lower left).

Supplementary Figure 2 – PDAC CSCs over-express DNMT1 and bear higher 5mC levels.

(A) Representative images of dot blots showing levels of 5mC in marker-positive (Fluo-positive and CD133-positive) versus marker-negative (Fluo-negative and CD133-negative) cells. Quantification of 5mC levels was performed by densitometry. **(B)** qRT-PCR analysis of DNMT1 in sorted PDAC-185 sphere-derived autofluorescent-positive (Fluo+) and -negative (Fluo–) cells (* P<0.05; n=4).

Supplementary Figure 3 – DNMT1 inhibitor Zebularine decreases CSC phenotype. (A)

Representative FACS plots for the CSC marker CD133 in spheres versus adherent primary PDAC cells. **(B)** mRNA levels for the pluripotency-associated gene NANOG in CD133+ vs CD133– sorted cells; n=4, * p<0.05. NANOG and DNMT1 protein expression in CD133+ and CD133– PDAC-354 sorted cells. Representative Western blot using β -ACTIN as loading control. **(C)** Graph illustrating cytotoxicity following 24h treatment with increasing concentrations of Zebularine; n=3, * p<0.05. **(D)** mRNA levels for DNMT1 gene in control (Ctrl) versus Zebularine (Zeb) treated cells n=3, * p<0.05. **(E)** Representative flow cytometry plots showing the percentage of Fluo+ cells from Control and Zebularine-treated cells (left), together with quantification (right). Data are represented as fold change compared to control cells; n=4, * p<0.05.

Supplementary Figure 4 – DNMT1 inhibitor Decitabine decreased CSC phenotype. (A)

Graph illustrating cytotoxicity following 24h treatment with increasing concentrations of Decitabine

(n=3, * $p<0.05$). **(B)** Representative Western blot showing DNMT1 protein level in control and Decitabine-treated spheres together with densitometric quantification. **(C)** Number of spheres per ml in 1st and 2nd generation cultures from various primary PDAC tumors (A6L, 185, and 354; * $P<0.05$, n=3). **(D)** qRT-PCR analysis of pluripotency-associated genes (NANOG, OCT3/4, SOX2, and KLF4) in 1st generation spheres. Data are normalized to β -ACTIN and presented as fold change compared to untreated cells, (* $P<0.05$, n=3). **(E)** Representative flow cytometry plots for E-CADHERIN and Pan-CYTOKERATIN (Pan-CK) in control and Decitabine-treated cells (upper panel) together with quantification (lower panel). Data are represented as fold change compared to control cells (n=4, * $p<0.05$).

Figure 5 – DNMT1 inhibitor Zebularine promotes CSC differentiation. **(A)** Representative images of pan-CYTOKERATIN (Pan-CK) staining for Ctrl versus Zeb-treated cells. **(B)** Representative flow cytometry plots for E-CADHERIN and Pan-CK surface expression in control and Zebularine-treated cells (left) together with quantification (right). Data are represented as fold change compared to control cells; n=4, * $p<0.05$. **(C)** Representative flow cytometry plots for Pan-CK surface expression in Cas9 only (control) and Cas9+sgDNMT1(DNMT1-KO) cells.

Supplementary Figure 6 – DNMT1 inhibition modulates expression of miR-203, miR-205, and the miR-17-92 cluster. **(A)** qRT-PCR analysis of miR-203 and -205 expression in control and Zebularine (Zeb)-treated cells. Data are normalized to Snord44 and presented as fold change compared to untreated cells. **(B)** qRT-PCR analysis of miR-203 and miR-205 in control (Cas9) and DNMT1-KO (Cas9+sgDNMT1) cells. Data are normalized to Snord44 and presented as fold change compared to control cells (n=4, * $p<0.05$). **(C)** qRT-PCR analysis of members of the miR-17-92 cluster (miR17, 18a, 19a, 19b, and 20a) in control and DNMT1-KO sphere-derived cells (* $p<0.05$, n=3).

SUPPLEMENTARY
MATERIALS & METHODS

Primary human cancer cells. The single cell-derived (SCD) tumor was generated by injecting a single autofluorescent positive CSC isolated from PDAC-185 (1). For in vitro studies, PDX tumors were minced, enzymatically digested with collagenase (Stem Cell Technologies, Vancouver, BC) for 60 min at 37°C and after centrifugation for 5 min at 1,200 rpm the pellets were resuspended and cultured in RPMI medium (Roswell Park Memorial Institute) supplemented with 10% fetal bovine serum (FBS) and 50units/mL penicillin/streptomycin.

Illumina methylation array. Total DNA was isolated using standard phenol-chloroform extraction. Bisulfite converted DNA was isothermally amplified at 37°C (20-24h). The amplified DNA product was fragmented by an endpoint enzymatic process. Fragmented DNA was precipitated, resuspended, and applied to an Infinium Human Methylation450K BeadChip (this array allows for the comparison of the DNA methylation status of 485,578 CpG loci across samples, covering all RefSeq genes at single-nucleotide resolution, microRNAs and differently methylated regions) and hybridized at 48°C (16-24h). During hybridization, the amplified and fragmented DNA samples anneal to specific oligomers covalently linked to the different bead types. The bead chips were then subjected to a single-base extension reaction. This reaction incorporates labeled nucleotides into the extended primers hybridized to DNA on the BeadChip. For methylation analysis, IDAT files were loaded into the R environment using the Bioconductor minfi package 3. The arrays were then background and control normalized using the minfi package. Technical differences between Infinium I and Infinium II probes were removed using Subset-quintile Within-Array Normalization, developed by Maksimovic et al. and available in the minfi package (2). The methylation status for each probe was recorded as a β -value.

Genomic region analysis. A probe was marked to be in a “promoter” region if it was located in the first exon, the 5' UTR, or a region up to 2 kbp upstream of the transcription start site (TSS) of any given transcript. Similarly, an “intragenic” probe was labeled if it was inside any intron or any exon other than the first. Intergenic probes were determined as those not falling into either of the two previous categories. A contingency table was built for each subset of probes and genomic regions,

with one variable indicating whether a given probe belonged or not to the subset, and the other indicating whether a given probe was labeled with the selected region. Significance of the association was determined by a Pearson's Chi-squared test with Yates' continuity correction. A significance level of 0.05 was used to determine whether a subset was dependent with respect to a given genomic region and an odds ratio was used as a measure of effect size.

CGI status analysis. The CGI locations used in the analyses were obtained from the R/Bioconductor package FDb.InfiniumMethylation.hg19 (R package version 1.0.1). The definition of CGI was done as described previously (3). Specifically, "CpG shores" were defined as the 2-kbp regions flanking a CGI. "CpG shelves" were defined as the 2-kbp regions either upstream of or downstream from each CpG shore. Probes not belonging to any of the regions previously mentioned were assigned to the category "non-CGI." Each probe was assigned to only one of the categories. In order to study the association between the given subset and the different CGI categories a 4-3-2 contingency table was constructed for every subset of probes. Firstly, a Chi-squared test was used to determine if any of the categories had a significant association with the given subset. Additionally, a 2-3-2 contingency table was defined and another Chi-squared test was used to independently evaluate the association of the given subset with each status level, a significance level of 0.05 being employed for all tests. Effect size was reported as the odds ratio for each of the individual tests.

AntagomiRs. The miR-17-92 cluster was knocked down using a mix of hsa-miR-17, 18a, 19a, 19b, and 20a antagomiRs (1.2 μ M each) or scrambled control. All antagomiRs were chemically synthesized as 2-O-methyl-oligoribonucleotide phosphorothioates containing cholesterol as modification of the 3' end to facilitate cellular uptake (BioSpring, Frankfurt, Germany).

Cell viability assay. Cells were seeded in 96-well plates (Nalgen Nunc International, Penfield, NY) at a concentration of 10^4 cells per well in 100 μ L of complete medium, allowed to attach for 24h and then treated with Zebularine or Decitabine for an additional 24h. Cytotoxicity was assessed using a bioluminescence-based Toxilight BioAssay assay following the

manufacturer's recommendations (Lonza, Basel, Switzerland). All the experiments were done in triplicates.

Apoptosis assay. Cancer cells and CSCs were plated at 3×10^5 cells/well in 6-well multi-well plates and cultured in the presence of Zebularine (75 μ M) for the indicated days. Attached and floating cells were collected, resuspended and stained for the CSC surface marker CD133 prior to staining with AnnexinV (550474) in AnnexinV binding buffer (556454; both from BD Pharmingen, San Jose, CA). Cells were then stained with DAPI and analyzed by flow cytometry.

Cell cycle analysis. Cells were trypsinized, washed in PBS, centrifuged, and pellets were fixed in 200 μ l of 70% ethanol and stored at -20°C until use. Cells were centrifuged and pellets resuspended in 200 μ l of PBS containing 10 μ g/mL of RNase A and incubated for 1h at 37°C. Cells were then stained with DAPI and analyzed by flow cytometry. For the identification of G0 quiescent population, cells were fixed in 70% ethanol at -20°C overnight, washed with PBS twice and stained with Ki67 (BD) for 30min at room temperature, followed by an additional wash with PBS. Cells were stained with DAPI to perform cell cycle analyses using a FACS CANTO II (BD) instrument.

Protein extraction and Western blotting. Cells were harvested in RIPA buffer (Sigma-Aldrich, St. Louis, MI) supplemented with a protease inhibitor cocktail (Roche Applied Science, Indianapolis, IN). The cell lysate was centrifuged at 14,000 rpm and the supernatant was collected. Protein lysates were quantified using a BCA Protein Assay Reagent kit (Pierce, Thermo Scientific, Waltham, MA). 50 μ g of protein was resolved by SDS-PAGE and transferred to nitrocellulose membranes (Amersham, Piscataway, NJ). Membranes were sequentially blocked with 1X TBS containing 5% BSA (w/v), or 5% (w/v) milk and 0.1% Tween20 (v/v), incubated with a 1:1,000 dilution of antibodies against NANOG (D73G4; Cell signaling); α -TUBULIN (#2144; Cell Signaling Tech, Danver, MA), β -ACTIN (Sigma-Aldrich), DNMT1 (D63A6; Cell signaling), and P21 (12D2; Cell Signaling) overnight at 4°C, washed three times with 1X PBS containing 0.1% Tween20 (v/v), incubated with horseradish peroxidase-conjugated goat anti-

rabbit or goat anti-mouse antibody (Sigma-Aldrich), and washed again to remove unbound antibody. Bound antibody complexes were detected with SuperSignal chemiluminescent substrate (GE Healthcare, Little Chalfont, UK).

RNA extraction and RT-qPCR. Total RNA was isolated by the guanidine thiocyanate method using standard protocols (4). One µg of purified RNA was used for cDNA synthesis using the QuantiTect Reverse Transcription Kit (Qiagen), followed by SYBR green RTqPCR using an Applied Biosystems 7500 real-time thermocycler (Applied Biosystems, Waltham, MA). Thermal cycling consisted of an initial 10min denaturation step at 95°C followed by 40 cycles of denaturation (15sec at 95°C) and annealing/extension (1min at 60°C). For miR analysis, 1µg of total RNA was reverse-transcribed using the NCode VILO miR cDNA synthesis kit according to the manufacturer's recommendations (Invitrogen, Waltham, MA). This step adds a polyadenylate tail to the miR population within the total RNA samples. The resulting cDNA was subjected to real-time PCR using SYBR Green ER qPCR Mix (Invitrogen). The Universal qPCR Primer was provided in the VILO kit and the forward primer for miR-17, 18a, 19a, 19b, 20a, 92a, 203, 205 Snord95 and Snord44 were purchased from Qiagen or Exiqon (Vedaaek, Denmark).

Gene	Primer sense	Primer antisense
NANOG	AGAACTCTCCAACATCTGAACCT	TGCCACCTCTTAGATTTCATTCTCT
OCT3/4	CTTGCTGCAGAAGTGGGTGGAGGAA	CTGCAGTGTGGGTTTCGGGCA
SOX2	AGAACCCCAAGATGCACAAC	CGGGGCCGGTATTATAATC
KLF4	ACCCACACAGGTGAGAAACC	ATGTGTAAGGCGAGGTGGTC
DNMT1	CAGGAAGAACGGCCGCAGCA	AGGCTTTGCCGGCTTCCACG
P21	AGTTCCTTGTGGAGCCGGAGC	GACATGGCGCCTCCTCTGAGT
TGFB2	CAACCACCAGGGCATCCA	TCGTGGTCCCAGCACTCA
ALK4	TGCAACAGGATCGACTTGAG	GGAGCGTCTTGTCTTGGAG
SMAD2	TCCCAGCAGGAATTGAGCCACA	GTTCTGCTGGAGAGCCTGTGTCC
SMAD4	CAGCACCACCCGCCTATGCC	TGGAACACCAATACTCAGGAGCAGG
CD133	CAGAGTACAACGCCAAACCA	AAATCACGATGAGGGTCAGC
BACTIN	GCGAGCACAGAGCCTCGCCTT	CATCATCCATGGTGAGCTGGCGG
C-MYC	CCCGCTTCTCTGAAAGGCTCTC	CTCTGCTGCTGCTGCTGGTAG

List of primers used for RT-qPCR

5mC quantification. Standard protocol was followed for the manual dot blot analysis. Briefly, DNA samples were diluted with TE buffer, denatured by heating to 99°C for 5min, chilled rapidly on ice and then loaded on a Hybond N+ nylon membrane (GE Health, Piscataway, NJ, USA). DNA was cross-linked using a Hoefer™ UVC 500 Ultraviolet Crosslinker (70,000 micro-joules/cm²). After crosslinking, membranes were blocked with 5% fetal bovine serum (BSA) for 1 h at room temperature, and then incubated with a polyclonal anti-5mC antibody (Active Motif, Carlsbad, CA, USA; #39649, 1:250) at 4°C overnight. 5mC was visualized by chemiluminescence. For quantification of 5mC we used the MethylFlash™ Methylated DNA Quantification Kit (Epigenetec; P-1034-96). In brief, 200 ng of DNA was added to the wells and subsequent quantification of 5mC was performed following the manufacturer's instructions.

CRISPR/Cas9-mediated knockout of DNMT1. In order to disrupt DNMT1, two sgRNAs targeting the CDS were designed according to <http://crispr.mit.edu>. Specific guide RNAs were synthesized as complimentary oligos, phosphorylated with T4 polynucleotide kinase (New England Biolabs), annealed, and cloned into the BbsI (New England Biolabs) site of pKLV-U6gRNA/BbsI-PKG-puro2A-BFP. The ligation mixture was transformed into OneShot chemically competent DH5alpha cells (Invitrogen). After plasmid DNA extraction (Qiagen), the sequence of the construct was verified by automated DNA sequence analysis. Replication-incompetent lentiviral particles, containing two different sgRNAs were produced in HEK293T following PEI-based transfection of cells with the packaging plasmids pCDNA3.1-VSV-G and pPAX2, as well as either one of the sgRNA plasmids. Forty-eight hours post transfection the medium was collected, cleared by low-speed centrifugation, filtered through 0.45µm pore-size PVDF filters, and stored in aliquots at -80°C. The viruses were subsequently titrated by flow cytometry analysis of BFP expression in 293T cells infected with increasing dilutions of virus. 185 PDAC cells stably expressing Cas9 were infected with viruses containing both DNMT1 sgRNAs at MOI=5 and selected with puromycin (1.5µg/ml) for 2 weeks. Loss of DNMT1 expression was confirmed by western blot analysis.

Sequences of CRISPR sgRNA used in this study:

NAME	sgRNA sequence (5'–3')
DNMT1 gRNA#1 (forward)	CACCGCGCTGCCCCGACGATGTCCGC
DNMT1 gRNA#1 (reverse)	TAAAACGCGGACATCGTCGGGCAGCGC
DNMT1 gRNA#2 (forward)	CACCGTGCCCCGACGATGTCCGCAGG
DNMT1 gRNA#2 (reverse)	TAAAACCCTGCGGACATCGTCGGGCAC

Immunofluorescence. Primary pancreatic cancer cells were seeded on cover slips in 6-well culture dishes (Corning, One Riverfront Plaza, NY) and treated with Zebularine. Following 7 days of treatment, cells were washed twice with 1X PBS, fixed with 4% formaldehyde for 10 min and blocked for 5 min with 10% heat inactivated normal donkey serum. After blocking, cells were permeabilized with 0.2% Triton X-100 for 10 min and incubated with the following antibodies: anti-Cytokeratin (CK3-6H5)-FITC (1:10, # 130-080-101 Miltenyi Biotec) and anti-E-Cadherin (1:50; # 610182 BD Biosciences). For E-Cadherin staining, cells were washed two times with 1X PBS and stained with Alexa-Fluor555-conjugated secondary antibody (1:500; # 558617 BD Biosciences). The nuclei of cells were stained with DAPI (5µg/ml; Sigma, St. Louis, MO) and cover slips were analyzed using an LSM-710 confocal microscope (Leica, Heidelberg, Germany).

Immunohistochemistry. For histopathological analysis, FFPE blocks were serially sectioned (3µm thick) and stained with hematoxylin and eosin (H&E).

SUPPLEMENTARY REFERENCES

1. Miranda-Lorenzo I, Dorado J, Lonardo E, Alcala S, Serrano AG, Clausell-Tormos J, et al. Intracellular autofluorescence: a biomarker for epithelial cancer stem cells. *Nat Methods* 2014;11(11):1161-9.
2. Maksimovic J, Gordon L, Oshlack A. SWAN: Subset-quantile within array normalization for illumina infinium HumanMethylation450 BeadChips. *Genome Biol* 2012;13(6):R44.
3. Wu H, Caffo B, Jaffee HA, Irizarry RA, Feinberg AP. Redefining CpG islands using hidden Markov models. *Biostatistics* 2010;11(3):499-514.
4. Chomczynski P, Sacchi N. Single-step method of RNA isolation by acid guanidinium thiocyanate-phenol-chloroform extraction. *Anal Biochem* 1987;162(1):156-9.